REPORT SERIES IN AEROSOL SCIENCE
N:o 237 (2021)

AEROSOL OPTICAL PROPERTIES, BLACK CARBON AND THEIR SPATIO-TEMPORAL VARIATION

KRISTA LUOMA

INAR – Institute for Atmospheric and Earth System Research
University of Helsinki
Helsinki, Finland

Academic dissertation

To be presented, with the permission of the Faculty of Science of the University of Helsinki, for public criticism in auditorium E204, Gustaf Hällströmin katu 2, on February 26th, 2021, at 13 o'clock noon.

Helsinki 2021

Author's Address: Institute for Atmospheric and Earth System Research / Physics
P.O. Box 64
FI-00014 University of Helsinki
krista.q.luoma@helsinki.fi

Supervisors: Professor Tuukka Petäjä, Ph.D.
Institute for Atmospheric and Earth System Research / Physics
University of Helsinki

Senior researcher Aki Virkkula, Ph.D.
Atmospheric Composition Research unit
Finnish Meteorological Institute

Reviewers: Associate Professor Nønne Prisle, Ph.D.
Nano and Molecular Systems Research Unit
University of Oulu

Robin Lewis Modini, Ph.D.
Laboratory of Atmospheric Chemistry
Paul Scherrer Institute

Opponent: Docent Andreas Petzold, Ph.D
Forschungszentrum Jülich GmbH
Insititute of Energy and Climate Research 8 - Troposphere

ISBN 978-952-7276-55-6 (printed version)
ISSN 0784-3496
Helsinki 2021
Unigrafia Oy

ISBN 978-952-7276-56-3 (pdf version)
http://www.FAAR.fi
Helsinki 2021

Acknowledgements

First, I thank Tuukka Petäjä and Aki Virkkula for supervising me during this four-year-long period. I always felt welcome visiting your offices! I am very grateful to Aki for sharing his knowledge about aerosol optics and black carbon. I appreciate all the guidance from our group leader Katrianne Lehtipalo, who also agreed to serve as the custos in the defense.

I thank Andreas Petzold for agreeing to be the opponent. I also thank Nønne Prisle and Robin Modini, who served as the pre-examiners of this thesis.

This research was conducted at INAR and I want to thank the director of INAR, Markku Kulmala, for giving me a chance to work in this great group. It has been motivating to work with research questions related to such an important topics as climate change and air quality.

This research would not have been possible without the INAR technical staff who have kept the measurements running. I especially want to thank Pasi Aalto, who has worked a lot with the set up of the aerosol optical instruments.

I appreciate the work of all the co-authors. I especially want to thank Jarkko Niemi from HSY for offering me the possibility to work with the black carbon data from the Helsinki metropolitan area. Working with Jarkko and the big data set taught me a lot of air quality, which was a rather new topic for me back then. Great thanks also to Liine Heikkinen, whose enthusiasm in atmospheric sciences is catchy and inspiring.

I have had great time with my group and colleagues at INAR! Thanks especially to Ilona, Meri, Magdalena, Sasu and Elisa for all the peer support. I also thank our regular lunch group that I have missed a lot during the pandemic. Thanks also to Laura Riuttanen for involving me in her climate education projects, which have been very interesting for me to work with alongside the thesis.

The amazing community of physics students made Physicum feel like home right in the beginning of my studies in 2011. I am happy that I got to start my studies with such a great bunch of students and that I met so many lovely people during my last ten years at UHEL. With you, I have had great discussions and even greater (and sometimes not so great) ideas! You have kept me sane with all the travels, festivals, get-togethers, climbing sessions, etc. You are very important friends to me and I want to thank you for all these great years! (I am not dropping names here, because the length of the list would be inappropriate…)

Finally, I thank my family for all the love and support. I am grateful to my parents for always encouraging me with my studies. I also thank my little sisters, Taija and Reetta, who always manage to cheer me up. Love you all!

I hope that I will soon get to see you all in person!

Krista Luoma
Helsinki, January 2021

Important abbreviations and nomenclature

Symbol	Typical unit	Explanation
ACI	*abbr.*	aerosol-cloud interaction
AOP	*abbr.*	aerosol optical property
ARI	*abbr.*	aerosol-radiation interaction
ATN	unitless	attenuation of light through filter sample
α, α_{abs}, α_{sca}	unitless	Ångström exponent, absorption Ångström exponent, and scattering Ångström exponent
*BC**	μg m^{-3}	black carbon
*BrC**	μg m^{-3}	brown carbon
b	unitless	backscatter fraction
C_{ref}	unitless	multiple scattering correction factor
*CCN**	cm^{-3}	cloud condensation nuclei
D_p	m	particle diameter
eBC	μg m^{-3}	equivalent black carbon
f(*Tr*)	unitless	filter loading correction for PSAP
k	unitless	imaginary part of the complex refractive index
λ	nm	wavelength
m	unitless	complex refractive index
MAC	g m^{-2}	mass absorption cross section
n	unitless	real part of the complex refractive index
*NR-PM1**	μg m^{-3}	non-refractory particulate matter/mass of particles smaller than 1 μm in diameter
OA	*abbr.*	organic aerosol
ω	unitless	single scattering albedo
PM	*abbr.*	particulate matter
PM_1, $PM_{2.5}$, PM_{10}*	μg m^{-3}	particulate matter/mass of particles smaller than 1, 2.5, and 10 μm in diameter
R(*ATN*)	unitless	filter loading correction for AE-31
*RF**	W m^{-2}	radiative forcing
RFE	W m^{-2}	radiative forcing efficiency (per unit of aerosol optical depth)
RH	%	relative humidity
*SOA**	μg m^{-3}	secondary organic aerosol
σ_{abs}, σ_{ATN}, σ_{ext}, σ_{sca}, σ_{bsca}	Mm^{-1}	absorption, attenuation, extinction, scattering and backscattering coefficient
Tr	unitless	transmission of light through filter

*The quantities and variables marked with a star are also used as abbreviations in this thesis and then they are written in roman and not in cursive.

Aerosol optical properties, black carbon and their spatio-temporal variation

Krista Hannele Luoma

University of Helsinki, 2021

Abstract

The amount and properties of atmospheric aerosol particles vary both in time and space depending on the proximity of the sources, atmospheric chemistry, and meteorological conditions. Atmospheric particulate matter worsens air quality and therefore affects human health. Aerosol particles have a notable effect also on the Earth's climate by scattering and absorbing the solar radiation and via aerosol-cloud interactions. The absorbing fraction of particles warms the climate, but due to the aerosol-cloud interactions and the greater fraction of scattering particles, the total effect of aerosols on the climate is cooling.

To determine the effect that particles have on the climate, it is crucial to know aerosol optical properties (AOPs) that describe the ability of atmospheric aerosol particles to scatter and absorb light at different wavelengths. The AOPs are determined by the size distribution, chemical composition, shape, and mixing state of the particles. This thesis aims to deepen the understanding of the AOPs and their relationships to the aerosol size distribution and chemical composition by combining comprehensive measurements of these parameters. The measurements were conducted at a rural boreal forest measurement site SMEAR II.

This thesis also studies the spatial and temporal variation of aerosols, by utilizing long-term aerosol measurements from different environments that vary from background sites to urban locations. The study of the spatio-temporal variation focuses on the variation in equivalent black carbon (eBC), which stands for optically measured black carbon (BC). A majority of the aerosol absorption is caused by BC, and therefore it represents the aerosol particles that have a warming effect on the climate. Since BC is emitted mainly by anthropogenic activities as a by-product of incomplete combustion, measurements of eBC give additional information on the health effects of aerosol particles since particles emitted from combustion sources are more harmful to health than aerosols from other sources. Studying the spatio-temporal variation in aerosol particles and especially in eBC concentration indicates the effect of anthropogenic activities on the aerosol concentration.

The measurements of the AOPs are rather robust, cheap and easy to run, which is why the AOPs are commonly measured properties. However, challenges arise with absorption and eBC measurements, which are typically measured by filter-based methods. In optical filter measurements, also the filter interacts with the radiation causing nonlinearities and uncertainties in the measurements. In addition to understand better the AOPs and the spatio-temporal variation in the atmospheric particles, this thesis aims to improve the filter-based measurements and to understand better the effect of different instruments and filter loading correction algorithms on the measured AOPs.

Keywords: ambient atmospheric aerosol particles, in-situ measurements, light absorption and scattering, long-term trends, temporal and spatial variation, filter-based absorption measurements

Contents

List of publications

This thesis consists of an introductory review, followed by five research articles. In the introductory part, the articles are cited according to their roman numerals. All the papers were reprinted under the Creative Commons Attribution 4.0 International License.

I **Luoma, K.**, Virkkula, A., Aalto, P., Petäjä, T., and Kulmala, M. : Over a 10-year record of aerosol optical properties at SMEAR II, *Atmos. Chem. Phys*., https://doi.org/10.5194/acp-19-11363-2019, 2019.

II **Luoma, K.**, Virkkula, A., Aalto, P., Lehtipalo, K., Petäjä, T., and Kulmala, M. : A comparison of three optical absorption photometers at a boreal forest site – effects of different correction algorithms, *Atmos. Meas. Tech. Discuss.,* https://doi.org/10.5194/amt-2020-325, in review, 2020.

III Heikkinen, L., Äijälä, M., Riva, M., **Luoma, K.**, Dällenback, K., Aalto, J., Aalto, P., Aliaga, D., Aurela, M., Keskinen, H., Makkonen, U., Rantala, P., Kulmala, M., Petäjä, T., Worsnop, D., and Ehn, M. : Long-term sub-micrometer aerosol chemical composition in the boreal forest: inter- and intra-annual variability, *Atmos. Chem. Phys*., https://doi.org/10.5194/acp-20-3151-2020, 2020.

IV **Luoma, K.**, Niemi, J.V., Aurela, M., Fung, P.L., Helin, A., Hussein, T., Kousa, A., Rönkkö, T., Timonen, H., Virkkula, A., and Petäjä, T. : Spatiotemporal variation and trends in equivalent black carbon in the Helsinki metropolitan area in Finland, *Atmos. Chem. Phys.*, https://doi.org/10.5194/acp-21-1173-2021, 2021.

V Kulmala, M., **Luoma, K.**, Virkkula, A., Petäjä, T., Paasonen, P., Kerminen, V-M., Nie, W., Qi, X., Shen, Y., Chi, X., and Ding, A. : On the mode-segregated aerosol particle number concentration load: contributions of primary and secondary particles in Hyytiälä and Nanjing, *Boreal. Environ. Res.*, 2016.

1 Introduction

Atmospheric aerosol particles are ubiquitous in the air surrounding us constantly and everywhere. Even though we inhale thousands of aerosol particles with every breath, it is easy to forget their existence since a majority of these particles are impossible to detect with a bare eye due to their very small size. Luckily, we are able to observe atmospheric aerosol particles and their properties with instruments that are sharper than our eyes (McMurry, 2000). This thesis reports measurements of the optical properties of atmospheric aerosol particles and studies how these properties vary within space and time.

Aerosol is defined as a mixture of gas and particles that can be either liquid or solid (Hinds, 1999). A typical example of aerosol is sprayed paint that has two simple components: the carrier gas and the liquid paint droplets. Atmospheric aerosols, however, are very different from aerosol sprayed out from a can. In the chaotic atmosphere, the size, concentration, chemical composition, and shape of particles are diverse and varying (Jimenez et al., 2009; Seinfeld & Pandis, 2016), which is the very opposite for the sprayed aerosol that is well-defined.

In the global scale, the biggest research questions in the field of aerosol physics are about the impacts of atmospheric aerosol particles on climate and air quality. The effect of particulate matter (PM) on the air quality is rather straightforward: increase in particulate pollution has adverse health effects on the human population. It has been estimated that in 2015, particulate pollution caused approximately 4.2 million premature deaths globally (Cohen et al., 2017). However, not all components of PM are equally harmful and the chemical composition affects the health effects of PM (Daellenbach et al., 2020). Whereas the effect of PM on the air quality is rather simple, the effect of aerosol particles on the climate and radiative forcing (RF) is much more complicated. PM affects the climate several ways: directly via aerosol-radiation interactions (ARIs; Charlson et al., 1992) and indirectly via aerosol-cloud interactions (ACIs; Lohmann & Feichter, 2005).

The complex ACIs and the versatility of atmospheric aerosols cause large uncertainties in predicting the climate effects of aerosols (Myhre et al., 2013). The amount of aerosols and their properties depend on the sources and ages of the particles, as well as on the dynamical and chemical processes in the atmosphere. Therefore, the properties of atmospheric particles vary substantially both in space and time. The variability is both short- and long-term as the aerosol loading varies diurnally and seasonally but it also changes in a long time scale as the emissions of particles change with anthropogenic activities or variations in the nature.

To observe both the spatial and temporal variations, measuring the aerosol particles and their properties in a long-term basis and in different locations are needed (Asmi et al., 2013; Collaud Coen et al., 2013; Laj et al., 2020). Aerosol measurements can be carried out either remotely or *in-situ*, which means that the measurements were carried out in the location of

interest from an air sample. Long-term in-situ measurements provide a good temporal coverage, but since one measurement represents just one location, in-situ measurements need to be conducted at various locations to reach better spatial coverage.

To determine the RF related to ARIs, measurements of aerosol optical properties (AOPs) are crucial (Haywood & Shine, 1995). AOPs describe the ability of aerosol particles to scatter and absorb light at different wavelengths and they depend on several factors, such as the size distribution, chemical composition, shape and mixing state of the particle population. In this thesis, the focus is on the in-situ measurements of aerosol scattering and absorption (i.e., AOPs). Measuring the scattering properties of aerosols is rather straightforward and the measurement uncertainties are already well known (Anderson et al., 1996; Anderson & Ogren, 1998). The absorption measurements, however, have turned out to be more challenging since these measurement typically apply filter-based methods, where the aerosol sample is collected in a filter medium (Moosmüller et al., 2009). Since also the filter interacts with the optical measurements, it causes some not-so-well defined uncertainties in the absorption measurements (e.g., Collaud Coen et al., 2010).

Despite the large uncertainties, one of the most interesting variable determined from the absorption measurements is the concentration of black carbon (BC), which has an important role in both global warming and poor air quality (Highwood & Kinnersley, 2006). BC is highly absorbing carbonaceous PM and it is emitted in the atmosphere as a by-product of incomplete combustion. Due to its absorbing nature, atmospheric BC has a warming effect on the climate. BC affects the climate also if it deposits on snow when it decreases the albedo of the snow surface and therefore enhances the melting of snow and ice sheets, which again, decreases the albedo of the Earth (Hadley & Kirchstetter, 2012). BC has actually been estimated to be the second largest individual anthropogenic warming agent (Ramanathan & Carmichael, 2008; Bond et al., 2013; Stocker et al., 2013). BC is also a health hazard since BC particles can act as carrier particles for toxic chemicals and inhaled BC particles can penetrate deep in the respiratory system and be transported further on to other organs (WHO, 2012). In general, BC gives additional information on the health effects of PM (Janssen et al., 2011) since PM originating from combustion, which BC is a by-product of, is more harmful to human health than PM originating from other sources (Krzyżanowski et al., 2005).

This thesis presents results on in-situ measurements of AOPs and BC concentration conducted at various environments. The focus is on measurements that were conducted at SMEAR II (Hari & Kulmala, 2005), which is a rural measurement site located in middle of a boreal forest in southern Finland. SMEAR II has comprehensive measurements on the AOPs, size distribution, and chemical composition, which are combined here in order to understand better the relationships between the AOPs and other parameters. Comprehensive measurements of absorption enabled to study also the challenges related to filter-based absorption measurements.

In addition to SMEAR II, this thesis includes measurements that were conducted in urban environments in Helsinki, Finland and in Nanjing, China. Comparing the measurement results between the different stations shows how the aerosol concentration and properties vary from a rural boreal forest to a traffic dominated urban site. Analysis on the long-term time series gave insight on the temporal variation in the aerosols.

In summary, the main aims of this thesis are:

- to understand better the links between the AOPs, size distribution and chemical composition and their relation to the sources of the particles (**Papers I, III, IV**)
- to quantify the spatial and temporal variations in aerosols and their properties (**Papers I, III–V**)
- to compare the different filter-based instruments and algorithms that are used to determine light absorption by aerosol particles (**Paper II**)

2 Atmospheric aerosol particles

The amount of particles, their size, chemical composition, shape and mixing state vary spatially and temporally. The variation is governed by the sources, atmospheric chemistry, and atmospheric dynamical processes (Seinfeld & Pandis, 2016). The abovementioned properties are important parameters since they determine, for example, the optical properties of the particles and their lifetime in the atmosphere. These factors are discussed in this chapter, which provides background information about atmospheric aerosol particles and presents the commonly used terms in the field of aerosol physics and aerosol optics.

Particulate matter (PM) is emitted in the atmosphere as primary or secondary particles; primary particles are already in their particulate form as they are emitted the atmosphere and secondary particles are formed in the atmosphere from gaseous pre-cursors. The sources of the particle and pre-cursor gases are both natural and anthropogenic (i.e., human related). Anthropogenic sources are typically linked to incomplete combustion processes that emit primary particles like black carbon (BC) (Paasonen et al., 2016), and pre-cursor gases, such as sulfur dioxide (SO_2), nitric oxides (NO_x), and volatile organic compounds (VOCs). Natural sources are manifold: wind blows primary dust particles from deserts or raises sea spray that generates salt particles; pre-cursor gases are emitted, for example by phytoplankton that emits dimethyl sulfide (DMS), and volcanoes that emit SO_2. Another example of natural sources are forests, where vegetation emits VOCs that participate in new particle formation (NPF; Ehn et al., 2014; Kulmala et al., 2013; Kulmala et al., 2004) and secondary organic aerosol (SOA) formation. Forest fires are also a notable source for aerosols and they can be either natural or anthropogenic. However, the ambient PM cannot be simply classified as primary or secondary, or as anthropogenic or natural origin. For example, secondary particles can be formed by combining pre-cursors gases from anthropogenic and natural sources, and pre-cursor gases can condense on the surface of a primary particle.

Especially primary particles, such as BC, mineral dust, salt from sea spray or biogenic pollen, can have very complex structures. For example, fresh BC particle is an agglomerate of several carbon spherules (Adachi et al., 2010), mineral dust and salt particles are crystalloids and biogenic particles can have very irregular and uneven surfaces (Li et al., 2020). Still, aerosol particles are typically assumed to be spherical since it is easier to apply equations and theories for round objects. This is a good assumption for secondary particles and liquid droplets. From now on, if not stated otherwise, term *particle diameter* assumes a diameter of a spherical particle.

The proximity of the sources and atmospheric dynamics determine whether the observed aerosol is fresh and locally emitted or aged and transported over long distances. The atmospheric dynamical processes can also dilute the aerosol or rain can scavenge the particles to the ground, which affects the amount of observed aerosol particles. The lifetime of particles in the atmosphere ranges from several hours to days or even to years, if the particles end up in the stratosphere, for example, by a volcano eruption (Deshler, 2008; Wagstrom & Pandis, 2009). The atmospheric dynamics affect the aerosol concentration on smaller and larger

scales. In smaller scale, the wind speed and variation in the boundary layer height has a notable role by mixing and diluting the air on a diurnal basis (Teinilä et al., 2019). In synoptic scale, the weather system determines whether the meteorological conditions are stagnant or if there are the long-range transport patterns or areas for wet removal of the particles.

Generally, the total amount of aerosols is reported by number concentration (N; i.e., the number of particles in a cubic centimeter) or by the particulate mass in a cubic meter of air. The particulate mass is typically reported for particles smaller than 1, 2.5, and 10 µm in diameter (PM_1, $PM_{2.5}$, PM_{10}). The highest concentrations of aerosol particles are measured in tightly packed megacities that are hot spots for bad air quality. For example, in Delhi, India, the average N is about 45 000 cm^{-3} and the mean $PM_{2.5}$ is about 120 µg m^{-3} (WHO, 2016; Gani et al., 2020). On the opposite, low concentrations are observed in areas that lack anthropogenic and natural sources. For example, Finnish Arctic sites reported on average N less than 1000 cm^{-3} (Laakso et al., 2003) and a site in Antarctica reported extremely low winter time median N as low as 15 cm^{-3} (Järvinen et al., 2013).

The sizes of the particles vary over five orders of magnitude as the size range of atmospheric aerosol particle diameter is typically defined to be from few nanometers to about 100 µm (Seinfeld & Pandis, 2016). The smallest particles are formed from clustered gas molecules. The largest particles are typically primary particles, such as pollen or grains of dust. In this study, the focus was on particles smaller than 10 µm.

The atmospheric aerosol size distribution is typically divided into five different modes that are formed by different dynamical and chemical processes. The modes are called the cluster (1.5 – 3 nm), nucleation (3 – 25 nm), Aitken (25 – 100 nm), accumulation (100 nm – 1 µm), and coarse (1 – 10 µm) modes (Kulmala et al., 2013; Seinfeld & Pandis, 2016). The particle size distribution is typically described by either a number or volume (or mass) distributions, which emphasize different modes. The cluster, nucleation and Aitken mode particles are high in number, but do not contribute significantly to the total volume (or mass) of the particles. Then again, the accumulation and coarse mode particles are high in volume (and mass) even though their number concentration is lower. The modes are typically simplified even more by talking about ultrafine (< 100 nm), fine (< 1 µm), and coarse (> 1 µm) mode particles.

The physical and chemical processes governing the aerosol size distribution are versatile. The cluster mode particles result from gas-to-particle conversion processes (Kulmala et al., 2013) but they can also originate as primary particles from traffic (Rönkkö & Timonen, 2019). The nucleation mode is dominated by NPF, where the pre-cursor gases form new particles by nucleation and growth processes (Kulmala et al., 2004; Kulmala et al., 2013). In the Aitken mode, the nucleation mode particles grow further by condensing vapors and coagulation (i.e., the particles collide and stick with each other). Particles in the Aitken mode range and larger can also be emitted in the atmosphere as primary particles. Accumulation mode particles are primary or formed mainly in cloud processing. In cloud processing, large enough particles (in the size range of tens of nanometers or larger; Kerminen et al., 2012) act as a cloud condensation nuclei (CCN) and form cloud droplets as water vapor condenses

on the CCN if the relative humidity (*RH*) reaches over 100 %. Chemical processes in the cloud droplets and their coagulation add up to the mass of the original CCN. If the cloud droplets do not rain but evaporate, the outcome is a larger processed particle than the original CCN. Due to the cloud processing there is typically a local minimum in particle size distribution between the Aitken and accumulation mode particles at around 100 nm that is known as the *Hoppel minimum* (Hoppel et al., 1990). The largest particles, which are the coarse mode particles, are typically primary: dust and sea salt particles, for example.

The removal of particles from the atmosphere is governed by evaporation, dry deposition, and wet deposition (Seinfeld & Pandis, 2016). If the conditions are not favorable for the growth processes of nucleation and Aitken mode particles, the particles may evaporate. Wet deposition means that the particles are scavenged from the atmosphere by rain so it mainly affects particles that act as CCN. Dry deposition means that the particles deposit on the ground or surfaces due to gravitation, which is more effective for larger particles.

In addition to the size distribution, one of the most important properties of the particles are their chemical composition. The chemical composition affects, for example, the hygroscopicity (ability to take up water vapor) of the particles, further on determining whether the particles can act as CCN. Hygroscopicity of the particles depends also on their size so that small particles are not as attractive for condensing water vapor than larger particles (Dusek et al., 2006). However, the chemical composition of the particles can increase their hygroscopicity when even smaller particles can act as a CCN.

According to their chemical composition, the particles are often classified to organic and inorganic particles. Organic aerosol (OA) contribute more to the PM (Zhang et al., 2007; Jimenez et al., 2009). OA consists of a complex mixture of different organic species (Seinfeld & Pandis, 2016): primary organic aerosols can be, for example, biogenic living micro-organisms, such as pollen, spores, bacteria or viruses; and secondary organic aerosol (SOA) is formed by pre-cursor gases (Ziemann & Atkinson, 2012), which are emitted by vegetation but also by anthropogenic combustion processes. Inorganic aerosol species, such as sulfate, ammonium, and nitrate, are typically linked to anthropogenic activities due to their main pre-cursor gas sources: SO_2 originates from industry and energy production; NH_3 from agriculture; and NO_x from industry and traffic (Aksoyoglu et al., 2017). However, not all inorganic species are from anthropogenic sources, for example, salt from sea spray, minerals from dust episodes, or sulfate aerosols originating from DMS emitted by phytoplankton.

Chemical composition is linked to the aerosol mixing state. Externally mixed particles are heterogeneous, which means that the chemical composition of the particles vary. Internally mixed aerosol means that the chemical composition of the particles is homogeneous so all the particles consist of the same chemical components (Seinfeld & Pandis, 2016). However, the chemical composition of the internally mixed particles themselves is necessarily not homogeneous, and the particle might have a separate core and coating (Lack & Cappa, 2010).

From the air quality perspective, the aerosol size distribution and chemical composition determine the toxicity of the particles, where the inhaled particles end up in the human respiratory system, and how they are transported in the human body (Valavanidis et al., 2008; Schraufnagel et al., 2019). For example, non-soluble ultrafine particles can end up to the alveoli where they can be transported in the blood circulation system and further on to the organs where the particles can accumulate. PM from combustion sources and especially from traffic have worse health effects than PM from other sources (Krzyżanowski et al., 2005) since traffic emits many toxic chemicals and heavy metals whereas wood combustion emits carcinogenic polycyclic aromatic compounds (Hellén et al., 2017; Rönkkö & Timonen, 2019). PM causes stress to the human body by accumulating in the organs and inducing inflammation. According to Cohen et al. (2017), air pollution is the fifth most important risk factors causing deaths globally and they estimated that 4.2 million deaths in 2015 were related to exposure to PM. Another estimation by Lelieveld et al. (2015) stated that PM caused 1.9 million pre-mature deaths in 2010. The main causes for PM related premature deaths are related to cardiovascular diseases, the second greatest cause were due to lung and respiratory diseases, and small fraction was caused by lung cancer (Lelieveld et al., 2015).

Apart from the health effects, the aerosol size distribution and chemical composition determines also their impact on the climate. Aerosol particles can affect the climate directly by scattering and absorbing solar radiation (i.e., aerosol-radiation interactions, ARIs). The direct effect is defined by the aerosol optical properties (AOPs), which again, are defined by the aerosol size distribution and chemical composition (Charlson et al., 1992). The AOPs and the direct effect of aerosols are discussed more in Sect. 2.1. Since cloud droplets could not be formed without CCN, aerosol particles also influence the climate via aerosol-cloud interactions (ACIs; Lohmann & Feichter, 2005).

Clouds have a considerable effect on the global albedo since they scatter light effectively back to space. The amount and properties of the CCN affect the formation, reflective properties, and lifetimes of the clouds and therefore they have a notable effect on the climate (Lohmann & Feichter, 2005; Stocker et al., 2013). The more there are CCN present in cloud formation, the more and smaller cloud droplets will form, which induces a cloud that has higher reflectivity than a cloud that has fewer larger droplets in it (Twomey, 1991). More CCN also increase the lifetime of the clouds since formation of rain from smaller cloud droplets takes more time (Albrecht, 1989). To conclude, more CCN increase the cooling effect of clouds since they reflect solar radiation longer and more efficiently back into space.

Aerosols affect the cloud formation also via a so-called semi-direct effect, which considers the effect of absorbing aerosols on the evaporation of the clouds and stability of the air column (Koch & Del Genio, 2010). Absorbing aerosols within the cloud layer can heat up the layer, which advances cloud evaporation. Absorbing aerosols can stabilize the air column by heating the upper layers and by cooling the lower layers as they prevent a fraction of the radiation from hitting the surface. Increased stability diminishes the convection and hinders cloud formation. The reduced convection in boundary layer also has an effect on the air quality since it reduces the mixing, boundary layer height, and dilution of pollutants

(Ding et al., 2016b). However, in some situations the presence of absorbing particles can even increase the cloud cover (Koch & Del Genio, 2010), which underlines the complexity and high uncertainty related to the semi-direct effect.

2.1 Aerosol optical properties

Aerosol optical properties (AOPs) describe the scattering and absorption by the particles at different wavelengths (λ). The AOPs depend on the concentration, size and chemical composition of the particles, and therefore the AOPs can also be used to retrieve some general information on these factors. AOPs are divided into extensive and intensive properties: the intensive properties are independent of the amount of aerosols and they only depend, for example, on the shape of the size distribution, and chemical composition, whereas the extensive properties depend also on the concentration of aerosol particles.

When a light beam travels through aerosol medium, its intensity attenuates due to extinction, which is the sum scattering and absorption caused by the particulate and gaseous components. Scattering and absorption are caused by the interaction between matter and electromagnetic radiation. In absorption, the energy of electromagnetic radiation is converted into heat, whereas, in scattering the incident light is diverted to different directions by reflection, refraction, and diffraction. The extinction, scattering, and absorption of light by a single spherical particle can be modelled by using Mie-theory that determines the extinction, scattering, and absorption efficiencies (Q_{ext}, Q_{sca}, and Q_{abs}) of the particle. The Q_{ext}, for example, is the relation between the extinction cross section (C_{ext}) to the physical cross section of the particle (A)

$$Q_{\mathrm{ext}} = \frac{C_{\mathrm{ext}}}{A}, \tag{1}$$

which applies also for the Q_{sca} and Q_{abs}. The Q_{ext} is calculated with a set of equations (presented e.g., by Seinfeld & Pandis, 2016) that depend on the particle diameter (D_{p}), the complex refractive index (m, see Eq. 9), and the wavelength (λ). The same analogy also applies to backscattering efficiency (Q_{bsca}), which describes the scattering that is directed to the backward hemisphere of the particle.

The Mie-theory applies the so-called size parameter (x) that combines the D_{p} and λ

$$x = \frac{\pi D_{\mathrm{p}}}{\lambda}. \tag{2}$$

The x is used to divide the scattering into three regimes, which are illustrated in Fig. 1. When the particles are significantly smaller than the λ ($x << 1$), the scattering is Rayleigh scattering; when the λ and the particle size are the same in magnitude ($x \approx 1$), the scattering happens in the Mie-regime; and when the particles are considerably larger than the λ ($x >> 1$), the scattering is geometric. In the Rayleigh regime, the Q_{sca} increases rapidly with increasing x and the scattering is equally or almost equally distributed in the forward and backward hemispheres (not seen in Fig. 1 due to linear y-axis). In the Mie-region, the situation is more complex and the Q_{sca} oscillates due to interference of the radiation inside the particle. As

the x increases, a greater fraction of the scattering is forwardly directed. The Q_{sca} is rather negligible in the Rayleigh regime, but starts to increase in the Mie-regime. In the geometric regime, the Mie-theory is no longer applicable since the scattering should be solved geometrically. As can be seen from Fig. 1, in linear scale, the Q_{sca} starts to increase around D_p ≈ 100 nm given a light wavelength of 550 nm. In practice this means, that for a particle to have notable optical signal in the visible wavelength range, the D_p should be around 100 nm or larger. Therefore, the aerosol particles discussed in this thesis are mainly larger than about 100 nm in diameter since they were optically measured at visible and near visible wavelengths.

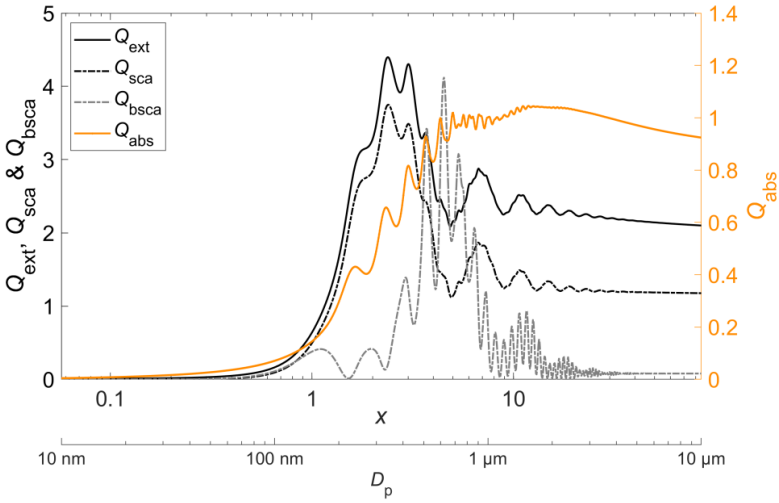

Figure 1: The dependency of the extinction, scattering, and absorption efficiencies (Q_{ext}, Q_{sca}, and Q_{abs}) on the size parameter (x) and particle diameter (D_p). The values were determined at 550 nm by using a complex refractive index m = 1.484 + 0.025i, according to Paper I.

To calculate, for example, the extinction of light by the whole aerosol population, the Q_{ext} values obtained from the Mie-theory for different sized particles, need to be integrated over the aerosol size distribution to obtain the extinction coefficient (σ_{ext})

$$\sigma_{ext}(\lambda) = \int Q_{ext}(x, m) \frac{\pi D_p}{4} \frac{dN}{d \log D_p} d \log D_p, \quad (3)$$

where the N is the number concentration of aerosol particles in a certain size bin. The same analogy functions also with scattering, backscattering, and absorption coefficients (σ_{sca}, σ_{bsca}, and σ_{abs}). These coefficients are typically reported for aerosol particles only, so the effect of the gaseous component is not included in these variables.

The unit of σ_{sca}, σ_{bsca}, σ_{abs}, and σ_{ext} is m^{-1}, but with atmospheric data, it is customary to use Mm^{-1} (i.e., 10^{-6} m^{-1}). The meaning of the abovementioned variables and their unit are the easiest to understand with the σ_{ext} and the Beer-Lamber-Bouguer law (Perrin, 1948)

$$I = I_0 \exp(-\sigma_{ext} L), \quad (4)$$

which describes the intensity of light (I) after a light beam, with original intensity of I_0, has travelled through aerosol medium over a distance L. Therefore, when the light beam has travelled a length that corresponds to σ_{ext}^{-1}, its intensity has decreased by a fraction of e^{-1}. Equation 4 is, for example, related to visibility, which is decreased by the scattering and absorption of aerosol particles (Koschmieder, 1924).

Considering the whole air column, from ground to the top of the atmosphere, the light attenuation by atmospheric aerosols is described by aerosol optical depth (δ), which in Eq. 4, replaces the product of $\sigma_{ext} L$ (integral of σ_{ext} from the ground level to the height of the air column L). The δ is an extensive property since apart from the properties of the particles it depends also on the aerosol burden in the whole column of air (Holben et al., 2001).

This thesis investigates the concentration of black carbon (BC), which is highly absorbing refractory carbonaceous material that is typically emitted as a by-product of combustion. Fresh BC particles consist of coagulated small carbon spherules ($D_p \approx 15$ nm; Zhang et al., 2008) that form complex agglomerate structures. In spoken language, BC is often referred as soot; however, scientifically spoken, soot contains also other material accumulated on the BC particles, such as organic carbon (OC).

Even though the term BC refers to chemical composition and not to optical properties it is described here next to the extensive AOPs since the concentration of *BC* is typically measured entirely by optical means (see Sect. 3.1.2). To emphasize the optical measurements, the measured *BC* concentration is hereon referred as *equivalent BC* (*eBC*) in line with the recommendation by Petzold et al. (2013). *eBC* means that the *BC* concentration was derived from σ_{abs} with a conversion factor called a mass absorption cross section (*MAC*).

$$eBC = \frac{\sigma_{abs}}{MAC}. \quad (5)$$

The *MAC* is actually an intensive AOP since it depends on the chemical properties, size, morphology, and mixing state of the aerosol particles and not their amount. If the *MAC* is considered a constant value, which is the case here, the *eBC* depends only on the σ_{abs}. However, in reality, the *MAC* varies spatially and temporally with different types of aerosols and it could be determined by comparing the σ_{abs} to the concentration of elemental carbon (*EC*), which is thermally measured concentration of refractory carbon

$$MAC = \frac{\sigma_{abs}}{EC}. \quad (6)$$

Variation in *MAC* means that a same amount of *EC* absorbs light differently due to different size, shape, mixing state, and chemical composition of the particles. For example, a large agglomerate, a large collapsed particle (former agglomerate), and a small individual carbon spherule absorb light differently compared to their mass (Bond et al., 2006). The situation is even more complex when a BC core gathers a coating that consists of purely scattering or just slightly absorbing material around the BC core. Typically, if liquid material condensates on a BC agglomerate, the agglomerate collapses and the particle forms a well structured sphere-shaped core and coating. The coating can enhance the absorption of the BC core by acting as a lens that gathers the light rays towards the core from a larger cross section (Bond

et al., 2006; Lack & Cappa, 2010). Using the term *eBC* instead of *BC* underlines that the measurements were possibly influenced by the abovementioned factors. The measurements of *eBC* concentration could be distorted also by other absorbing material than BC, such as, dust (Fialho et al., 2005), humic-like substances, and brown carbon (BrC; Andreae & Gelencsér, 2006). BrC refers to OC species that absorb light mainly at wavelengths shorter than 600 nm (Kirchstetter et al., 2004; Andreae & Gelencsér, 2006).

Like *MAC*, all the AOPs depend on the λ of the radiation. The wavelength dependency of an optical property σ is described by an Ångström exponent (α; Ångström, 1929)

$$\alpha = -\frac{\ln\frac{\sigma_{\lambda_1}}{\sigma_{\lambda_2}}}{\ln\frac{\lambda_1}{\lambda_2}}. \quad (7)$$

The α can be determined for several AOPs and in this thesis the α was calculated for σ_{sca} and σ_{abs} to obtain the α_{sca} and α_{abs}, respectively. In general, the σ_{sca} and σ_{abs} decrease with longer λ. The α_{sca} depends on the relation between the particle size and the λ of the radiation. In the Rayleigh regime, the α_{sca} approaches four and with increasing particle size, the α_{sca} decreases. Apart from the particle size, the chemical composition has an effect on the α_{abs}. For example, in the presence of BrC, the σ_{abs} at short wavelengths is emphasized, which increases the α_{abs} (Andreae & Gelencsér, 2006). Similarly to the *MAC*, the possible core-coating-structure also has a great effect on the α_{abs} (Lack & Cappa, 2010). The α_{abs} is commonly used to determining the source of BC by the so-called Aethalometer model, which assumes that BC has two sources: traffic or biomass burning (Sandradewi et al., 2008; Drinovec et al., 2015; Zotter et al., 2017).

The single scattering albedo (ω) describes the scattering fraction of the σ_{ext}

$$\omega = \frac{\sigma_{sca}}{\sigma_{ext}} = \frac{\sigma_{sca}}{\sigma_{sca}+\sigma_{abs}}. \quad (8)$$

The higher the ω, the more efficient scatterers the particles are. Then again, particles with low ω absorb relatively more light and are darker in color. The ω gives some insight about the chemical composition of particles, for example, low ω indicates that the particles consist of a higher fraction of BC.

The complex refractive index (m) was already mentioned when discussing about the Mie-theory. The m consists of a real (n) and imaginary (m) part

$$m = n + ik, \quad (9)$$

which describe the scattering and absorption properties of the particles, respectively. Like the ω, the m depends on the chemical composition of particles.

The backscatter fraction (b) is the relation between the σ_{bsca} and σ_{sca}

$$b = \frac{\sigma_{bsca}}{\sigma_{sca}}. \quad (10)$$

Like the α_{sca}, also the b depends on the size distribution. For gas molecules and particles in Rayleigh regime the b is 0.5, because for particles that are considerably smaller than the wavelength the scattering in forward and backward hemisphere is equal. For larger particles,

the b decreases, because larger particles scatter light more efficiently in the forward direction. The size dependency of the b differs somewhat from that of the α_{sca} since the α_{sca} is more sensitive for coarse mode particles. The b is typically linked to the upscatter fraction β (Delene & Ogren, 2002), which is related to the ability of aerosols to scatter solar radiation back in space (see Eq. 13). The β can be estimated by

$$\beta = 0.0817 + 1.8495b - 2.9682b^2. \quad (11)$$

The β increases with the b, meaning that smaller particles scatter solar radiation more efficiently back to space. Also, the asymmetry parameter (g) is sometimes determined by using the b. According to Andrews et al. (2006),

$$g = -7.14b^3 + 7.46b^2 - 3.96b + 0.9893. \quad (12)$$

Theoretically, the g varies from -1 to 1 so that when g = -1 all the scattering is to the backward direction and when g = 1 all the scattering is to the forward direction.

The final intensive AOP is the radiative forcing efficiency (*RFE*), which is related to the ARIs. The effect of ARIs on the climate is called the direct effect and it describes how the scattering and absorption by aerosol particles influences the radiative forcing (RF). Due to the great scattering fraction of aerosols, the total effect of ARIs on the global RF is negative. However, the absorbing fraction of aerosol, which is mainly caused by BC, has a considerable warming effect and it is actually been estimated as the second strongest agent in global warming (Ramanathan & Carmichael, 2008; Bond et al., 2013; Stocker et al., 2013). The efficiency of the aerosol particles to decrease or increase the RF is described by the radiative forcing efficiency (*RFE*), which reports the RF that the particles would have per unit of aerosol optical depth (δ) (Sheridan & Ogren, 1999)

$$RFE = \frac{RF}{\delta} = -S_0 D T_{at}^2 \omega \beta (1 - A_c)\left[(1 - R_S)^2 - \left(\frac{2R_S}{\beta}\right)\left(\frac{1}{\omega} - 1\right)\right]. \quad (13)$$

The δ is an extensive AOP that describes the attenuation of light by aerosol particles in a column of air. The *RFE* depends on the environmental factors that are the solar constant (S_0), fractional day length (D), atmospheric transmission (T_{at}), cloud fraction (A_c), and surface reflectance (R_S). Suitable and generally used values for the environmental parameters are presented by Haywood and Shine (1995) and discussed more by **Paper I**. In Eq. 13, the properties of the aerosols are described by the ω and β. The *RFE* can be either positive or negative, depending mainly on the relationship between the ω and R_S; for example, dark particles above reflective surface (e.g., BC on snow) have a warming effect, and highly scattering particles above dark surface (e.g., dust above sea) have a cooling effect.

3 Measurements and methods

Papers I–V apply data from several stations measured by various in-situ instruments. This chapter presents the most relevant instruments, measurement sites, and data analysis methods used in this thesis.

3.1 Instrumentation

This section presents the instrumentation the study used to measure AOPs and *eBC* concentration. Measurements of the σ_{sca}, σ_{bsca}, and σ_{abs} were the main topic in **Paper I**; and the measurements of *eBC* concentration (i.e., σ_{abs}) were discussed in **Papers II–V**. In addition, **Papers I** and **V** applied data of the aerosol size distribution and **Paper III** of the aerosol chemical composition, and therefore the instrumentation to measure the aerosol size distribution and chemical composition are also described shortly. Different papers also utilized data of meteorological parameters, $PM_{2.5}$ concentration, and concentrations and mixing ratios of gaseous components, but those measurements are not described here as they are not the main topic of this thesis.

3.1.1 Scattering measurements

The σ_{sca} and σ_{bsca} are commonly measured by an integrating nephelometer. The development of the nephelometers began already several decades ago (Beuttell & Brewer, 1949; Crosby & Koerber, 1963; Charlson et al., 1967). Due to the long period of development, their problematics and uncertainties are well known (Anderson et al., 1996; Anderson & Ogren, 1998). Here, we present the operating principle of TSI Incorporated integrating nephelometer model 3563 (hereon referred ad TSI 3563; Anderson et al., 1996), which is, unfortunately, no longer in production. However, the measurement principle of the TSI 3563 is similar, for example, to the still-manufactured Aurora series by Ecotech (Müller et al., 2011).

The three main parts of the TSI 3563 are a measurement cell, light source, and detector. The aerosol sample flows through the cell so the instrument measures particles that are suspended in air. In the cell locates the measurement volume, which is illuminated with white light. The light is diffused so that its intensity follows the Lambertian cosine law (i.e., the intensity is proportional to the cosine of ε, where the ε describes the angle from the light source). All the surfaces inside the instrument are black and highly absorbing, so in ideal condition (i.e., perfectly absorbing surfaces without contamination) the only material scattering the light is the PM in the measurement volume. The scattered light is detected by a photomultiplier tube that counts photons at certain wavelengths, which in the TSI 3563 are 450, 550, and 700 nm. The alignment of the detector and light source form a right angle, which enables detecting the scattering from different angles at the same time. Therefore, the instrument integrates the scattering from the scattering angle (θ) 0° to 180° geometrically,

which is the reason why the instrument is called *integrating* nephelometer. This can be demonstrated with an equation

$$\sigma_{\mathrm{sca}} = 2\pi \int_0^{\pi} \zeta(\theta) \sin(\theta)\, \mathrm{d}\theta, \tag{14}$$

where the ζ is the scattering phase function, which describes the scattering intensity at different angles. When the whole sample volume is illuminated, the instrument measures the scattering from all angles and determines the σ_{sca}. To determine the σ_{bsca}, the half of the measurements volume that represents the forward scattering (i.e., $90° < \theta < 180°$), is shadowed, so the detector observes only the backscattered light.

Due to geometrical challenges, the geometrical integration is not perfect and the TSI 3563 can only detect scattered light from the range of 7° – 170°. This is fixed by a truncation correction, which depends on the scattering phase function, which again depends on the size distribution, shape, mixing state, and refractive indices of the particles The truncation correction estimates the scattering on the blind angles typically by applying the α_{sca} and multiplicatively applies it to the σ_{sca} and σ_{bsca} (Anderson & Ogren, 1998; Bond et al., 2009; Müller et al., 2011).

Since the σ_{sca} and σ_{bsca} describe the scattering of aerosol particles only, the scattering by gas molecules has to be omitted in the measurements. This is considered by filtering out the PM from the sample air regularly and subtracting the scattering of filtered air from the total scattering. This procedure also considers the scattering from the walls and impurities accumulated in the cell. The instrument is calibrated with a gas that has a well known scattering properties, such as CO_2.

3.1.2 Absorption and equivalent black carbon measurements

There are several instruments available to measure the σ_{abs}. Here, the σ_{abs} and *eBC* concentration measurements were conducted by three different instruments: an aethalometer (model AE-31 by Magee Scientific), a Particle Soot Absorption Photometer (PSAP; model 3-λ by Radiance Research), and a multi-angle absorption photometer (MAAP; model 5012 by Thermo Scientific Inc.). Hereon the aethalometer is referred as AE-31, to avoid confusion with the newer upgraded aethalometer model AE-33. Whereas the integrating nephelometer that measures particles that are suspended in the air, the absorption photometers are based on collecting the sample particles on a filter, which is the main cause for the uncertainties related to the absorption measurements. The filter in optical measurements is problematic since in addition to the PM, also the filter fibers interact with the radiation, which affects the measurements. Before a further discussion of the challenges related to the filter-based methods, this section presents the basic principles of the absorption photometers.

The operating principals of the PSAP and AE-31 are very similar (Bond et al., 1999; Weingartner et al., 2003). They measure the σ_{abs} at several wavelengths: PSAP operates at three wavelengths (467, 530, and 660 nm) and the AE-31 at seven wavelengths (370, 470, 520, 590, 660, 880, and 950 nm). To be precise, the PSAP and AE-31 measure the attenuation coefficient (σ_{ATN}; or in some occasions the *uncorrected absorption*, σ_0) and not the σ_{abs},

which is a derivative of the σ_{ATN}. An equation for the σ_{ATN} is derived from the Beer-Lambert-Bouguer law (Eq. 4)

$$\sigma_{ATN} = \frac{1}{L}\ln\left(\frac{I_{t-\Delta t}}{I_t}\right) = \frac{A_{\text{spot}}}{Q\Delta t}\ln\left(\frac{I_{t-\Delta t}}{I_t}\right), \tag{15}$$

where A_{spot} is the area of the sample spot, Q is the sample flow, Δt is the length of the measurement period, and the $I_{\Delta t - t}$ and I_t are the measured light intensities through the filter in the beginning and in the end of the measurement period. I through the filter gradually decreases as the filter gets loaded with particles. The loading of the filter is described by the attenuation (ATN) and transmission (Tr)

$$ATN = \ln\left(\frac{1}{Tr}\right) = \ln\left(\frac{I_0}{I_t}\right), \tag{16}$$

where the I_0 is the light intensity through a pristine filter. The custom is to use the ATN with aethalometer and the Tr with PSAP measurements. As the filter gets loaded with particles, the ATN and Tr responses are the opposite: ATN increases and Tr decreases.

The σ_{ATN} does not take into account the interaction of radiation with the filter material nor attenuation of light due to scattering of the particles and therefore the σ_{ATN} does not represent the light absorption by particles. These issues are considered when the σ_{abs} is derived. In the AE-31 measurements, the σ_{abs} is typically derived as following

$$\sigma_{\text{abs}} = \frac{\sigma_{ATN} - a_s\sigma_{\text{sca}}}{C_{\text{ref}}R(ATN)}, \tag{17}$$

where the scattering by the aerosol particles ($a_s\,\sigma_{\text{sca}}$) and the filter effect ($C_{\text{ref}}\,R(ATN)$) are taken into account. Scattering in the filter medium lengthens the optical path of the incident radiation and the probability for a photon to be absorbed by a particle increases. Therefore, the scattering by particles induces apparent absorption, which is considered by reducing a fraction a_s of σ_{sca}. The filter fibers also scatter light, which is called multiple scattering. This is taken into account with the multiple scattering correction factor (C_{ref}) that is typically considered a constant value larger than unity. When PM accumulates in the filter medium, the optical path of the incident radiation gradually decreases and the particles absorb relatively less light. Therefore, the response of the instrument decreases with increasing filter loading. This nonlinearity is amended with a filter loading correction ($R(ATN)$) that depends on the ATN. Even though, in theory, the C_{ref} should depend only on the filter material used, it has been observed that the C_{ref} varies both spatially and temporally (Collaud Coen et al., 2010; Backman et al., 2017). The C_{ref} can be determined by comparing a reference σ_{abs} ($\sigma_{\text{abs,ref}}$) to an σ_{ATN} that was corrected for the filter loading error:

$$C_{\text{ref}} = \frac{\sigma_{ATN}}{\sigma_{\text{abs,ref}}R(ATN)}. \tag{18}$$

The C_{ref}, a_s, and $R(ATN)$ have been a subject to many studies and there has been several suggestions for correction algorithms. The algorithms proposed different constants for the coefficients and different types of filter loading corrections (Weingartner et al., 2003; Arnott et al., 2005; Schmid et al., 2006; Virkkula et al., 2007; Collaud Coen et al., 2010; Li et al., 2020). Some of the correction algorithms are presented in detail in **Paper II**. In general,

there has not been a common consensus on the most accurate correction algorithm. Database for ACTRIS (Aerosols, Clouds and Trace gases InfraStructure) data, for example, asks to submit the σ_{abs} that was measured by an AE-31 so that the data was not treated by the filter loading correction nor the subtraction of particle scattering subtraction, and that applied a constant $C_{ref} = 3.5$.

The newer aethalometer model AE-33 has a rather similar measurement principle to the AE-31. However, it measures the σ_{ATN} of two sample spots that have different flows and it applies a so-called dual-spot correction algorithm to determine σ_{abs} (Drinovec et al., 2015).

The PSAP suffers from the same problems as the AE-31 and to obtain the σ_{abs}, the σ_{ATN} needs to be corrected. A common correction used for the PSAP data is

$$\sigma_{\mathrm{abs}} = 0.85 \cdot \frac{1}{K_2}(f(Tr)\sigma_{ATN} - K_1\sigma_{\mathrm{sca}}), \tag{19}$$

where the coefficients K_1 and K_2 are 0.02 and 1.22, respectively. Equation 19 was suggested by Bond et al. (1999) and it was later revisited by Ogren (2010). The PSAP correction algorithms also take into account the scattering by the particles and the filter fibers as well as the nonlinearity caused by the filter loading. Virkkula (2010) suggested an alternative algorithm to obtain the σ_{abs} from PSAP measurements and it is presented in **Paper II**.

The operating principle of the MAAP differs from that of PSAP and AE-31 by two factors: firstly, in addition to *Tr* through the filter, the MAAP measures backscattered light from the filter at two different angles; and secondly, the MAAP does not determine the σ_{abs} as in Eqs. 15, 17, or 19, but it applies a so-called two-stream approximation in radiative transfer model in determining the σ_{abs} (Petzold & Schönlinner, 2004). These differences in the MAAP make it more precise and less sensitive to the filter artefacts than the PSAP or AE-31 and therefore MAAP is typically used as a reference instrument for the σ_{abs} measurements (e.g., as $\sigma_{abs,ref}$ in Eq. 18). MAAP, however, operates only at one wavelength (637 nm), so it cannot be used in determining the wavelength dependency of σ_{abs} (i.e., α_{abs}).

As already discussed in Sect. 2.1, the concentration of *eBC* is typically derived from the σ_{abs} measurements by applying a constant *MAC* value (Eq. 5). The *eBC* concentration can also be derived from the σ_{ATN} in a similar manner to Eq. 5, but by replacing the σ_{abs} by the σ_{ATN}, and the *MAC* by a mass attenuation cross section (M_{ATN}). Since there are many possibilities to determine the σ_{abs} and *eBC* concentration, it is important to report which instrument and algorithm (or no algorithm) were used, and what constants were used for the a_s, C_{ref}, *MAC*, or M_{ATN}.

3.1.3 Size distribution and chemical composition measurements

The aerosol size distribution were measured by three instruments: at SMEAR II a Twin Differential Mobility Particle Sizer (TDMPS; Aalto et al., 2001) and an Aerodynamic Particle Sizer (APS; TSI model 3321) were used; and at SORPES a flow-switching-type DMPS was operated (Qi et al., 2015). The TDMPS operated in the size range of 3 – 1000 nm, the flow-switching-type DMPS in the range of 6 – 800 nm, and the APS in the size range of 0.5

– 20 µm. The APS uses aerodynamic D_p, which was converted to geometric D_p by assuming an average density of 1.5 g cm^{-3} for the particles (Kannosto et al., 2008). More detailed descriptions of the size distribution measurements are presented in **Paper I**.

The chemical composition of non-refractory PM_1 (NR-PM_1) was measured by an Aerosol Chemical Speciation Monitor (ACSM; Aerodyne Research Inc.). The ACSM reports the concentrations of particulate ammonium, nitrate, sulfate, chloride, and organic species. Since the instrument only detects the non-refractory composition, it is not able to measure refractory components, such as *EC*, minerals, or sea salt. A more detailed description of the instrument is provided in **Paper III**.

3.2 Measurement sites

The measurements included in this thesis were conducted at three different main locations: at SMEAR II in Hyytiälä, Finland; at 14 air quality stations in the Helsinki metropolitan area (HMA), Finland; and at SORPES station, in Nanjing, China. Data collected at SMEAR II were studied in all the **Papers I–V**. The measurements in the HMA were discussed in **Paper IV** and the measurements at SORPES were studied in **Paper V**.

3.2.1 SMEAR II

SMEAR stands for Station for Measuring Ecosystem-Atmosphere Relations. SMEAR stations form a network of comprehensive atmosphere measurement sites (Hari & Kulmala, 2005). SMEAR II is the most comprehensive site of the SMEAR network as there are more than thousand environmental parameters measured and recorded on a long-term basis. The site was founded in 1995 and it has been operational ever since. SMEAR II is also part of large-scale measurement networks such as ACTRIS, LTER-Europe (Long-Term Ecosystem Research in Europe), and ICOS (Integrated Carbon Observation system).

SMEAR II it is located in Hyytiälä, in southern Finland (61°51’ N, 24°17’ E, 181 m a.s.l., Fig. 3). The station is situated in the middle of a boreal forest that consists mostly of scot pine trees (*Pinus sylvestris* L.) and therefore it represents boreal forest environment. In **Paper IV**, SMEAR II was classified as a regional background site to match the categories used in the study. However, in reality and according to the Global Atmospheric Watch (GAW) classifications, SMEAR II is a rural background station. There are no significant pollution sources nearby except for sawmills that are located about 6 km southeast. The nearest cities are Tampere (population: 220 000) and Jyväskylä (population: 140 000) that are located in about 60 and 100 km distance. Otherwise, the regional area is sparsely populated.

The data availability of the most relevant instruments regarding this thesis are presented in Fig. 2. The scattering was measured by a TSI 3563, and the absorption by an AE-31, a PSAP, and a MAAP. The size distribution was measured by a DMPS and APS, and the chemical composition of NR-PM_1 by an ACSM. The start of the DMPS measurements date to year 1995, however, here only the data that was measured in parallel with the AOPs were

considered. Detailed data availability of the nephelometer and AE-31 are presented in the supplementary material of **Paper I**. The measurement line of the instruments that measured AOPs is described in detail in **Paper II**. The most important notion is the change in the cut-off size of the AOP measurements in June 2010. When the measurements of the AOPs were started, the measurements were conducted only for PM_{10}. However, in 2010 the cut-off size of the inlet was upgraded so that it alters every 10 minutes between 1 and 10 µm so also the AOPs of PM_1 were measured.

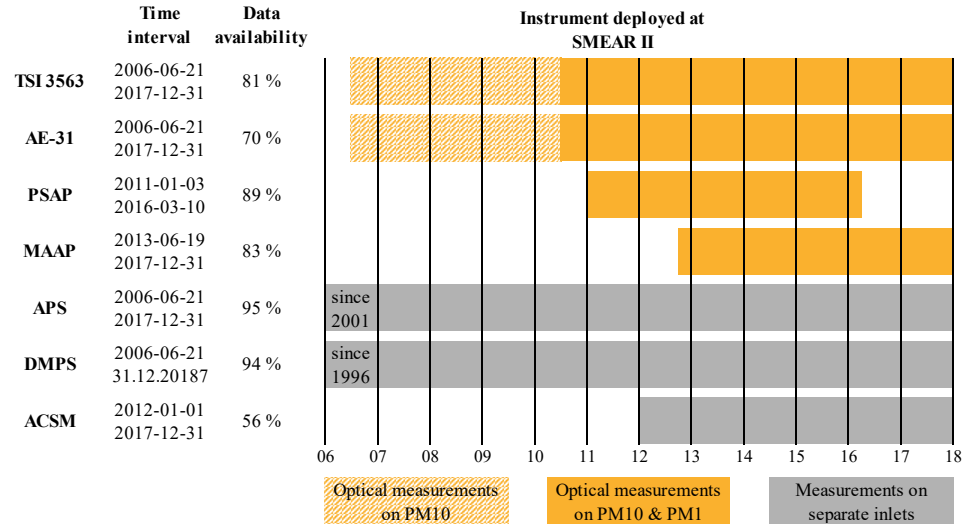

Figure 2: Diagram of the measurement times and data availability at SMEAR II. The orange bars are the measurements of AOPs. The lighter color indicates the time when only the AOPs of PM_{10} were measured, and the darker orange indicates the time when the AOPs were measurements for both PM_1 and PM_{10}. The gray bar shows the size distribution and chemical composition measurements that had their own individual inlets. The data availability is calculated for the reported time interval.

3.2.2 Helsinki metropolitan area

The HMA consists of four cities (Helsinki, Espoo, Vantaa, and Kauniainen) with a total population of about 1.4 million. The HMA is located in the southern part of Finland on the coast of the Baltic Sea. In the HMA, data from 14 sites were included in the study and their locations are presented in Fig. 3. These sites were classified into four categories that were traffic sites (TR), detached housing areas (DH), urban background (UB), and regional background sites (RB). Six of the sites were categorized as TR, five as DH, two as UB, and one as RB. Detailed information and locations of the sites are reported in **Paper IV**. All but one of the sites were air quality monitoring stations run by the Helsinki Regional Services Authority (HSY), and one of the sites was SMEAR III, which is run by the Institute for Atmospheric and Earth System Research (INAR) and Finnish Meteorological Institute (FMI). The

measured parameters in the HMA were *eBC*, $PM_{2.5}$, and NO_x concentrations. The *eBC* concentrations in the HMA were mainly measured by MAAPs, but some sites operated the newer aethalometer model (AE-33).

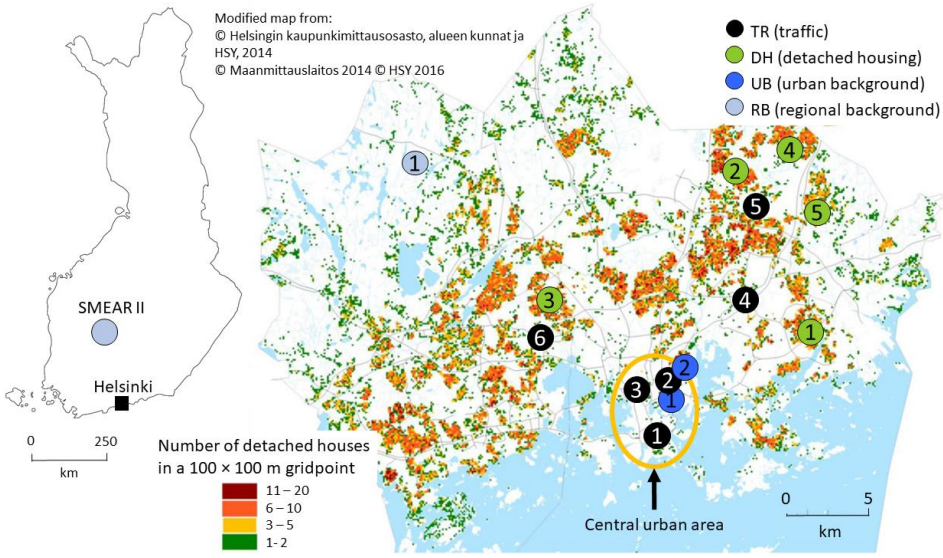

Figure 3: Stations located in the HMA and the location of SMEAR II. The color coding and numbering of the markers indicate the site classification and station names used in Paper IV. Modified from Fig. 1 in Paper IV.

3.2.3 SORPES

Station for Observing Regional Processes of the Earth System (SORPES) locates in a Chinese megacity, Nanjing, with a population of about 8.5 million. SORPES acts as a regional background site for the Yangtze River Delta area, which is a highly industrialized area with more than 100 million inhabitants. SORPES was founded in 2011 and the station is situated about 20 km northeast from the Nanjing city center (32°07' N, 118°57' E, 40 m a.s.l.). The SORPES is considered as a background site with little local influence; depending on the wind conditions, the station might observe pollution from the center of Nanjing and the nearby highway (Ding et al., 2016a). The *eBC* concentration at SORPES was measured by an AE-31 and the size distribution by a flow-switching-type DMPS.

3.3 Data analysis

This section presents data analysis tools and methods that were used to analyze the long-term trends in **Papers I** and **IV**, to determine the complex refractive index (*m*) in **Paper I**, and to estimate the numbers of primary and secondary aerosols in **Paper V**.

3.3.1 Long-term trend analysis

The Mann-Kendall (MK) test and Sen's slope estimator are non-parametric methods that allow missing values and therefore, they are suitable methods for analyzing environmental data such as long-term measurements of the AOPs. The MK test reports if a long-term trend in a studied variable is statistically significant and whether it is monotonically decreasing or increasing. Sen's slope estimator, again, estimates the magnitude of the trend. This section describes shortly the MK test and the Sen's slope estimator based on Gilbert (1987).

Seasonal variation in environmental data can lead to autocorrelation (i.e., a high value is followed by yet another high value and vice versa), which is not accepted by the MK test. Therefore, the trend analysis applied a *seasonal* MK test and *seasonal* Sen's slope estimator that are variations of the original MK test and Sen's slope estimator and that overcome the autocorrelation problem related to the seasonality of the data. Here the word *seasonal* refers to any cyclic pattern and not just the changing season of a year. The seasonality could also be caused, for example, by diurnal patterns of boundary layer dynamics or traffic rates.

The normal MK test determines whether the time series have a statistically significant trend or not. First, the test determines the differences between all the given data points in the order they were measured. Then the test computes the MK statistics (S) that is the sum of the signs of the all the differences between the data points (i.e., number of positive differences minus the number of negative differences). Positive S means that the value increased over time and vice versa. The S is used to calculated the test statistics (Z) as following:

$$Z = \frac{S-1}{\sqrt{\mathrm{VAR}(S)}}, \text{if S} > 0, \tag{20}$$

$$Z = \frac{S+1}{\sqrt{\mathrm{VAR}(S)}}, \text{if S} < 0. \tag{21}$$

The VAR(S) is the variance of S that takes into account the data ties (see Gilbert, 1987). In case the $S = 0$, the $Z = 0$ as well. The null hypothesis (H_0) is *no trend* against the alternative hypothesis (H_A), which is set up by the S (or Z): if the S (or Z) is positive the H_A is *increasing trend*, and if the S (or Z) is negative the H_A is *decreasing trend*. The H_0 is rejected, if the probability value is lower than the set up significance level s. The probability values are retrieved from a standard normal statistical table that reports the probabilities of a cumulative normal distribution.

The magnitude of the trend can be determined, for example, with the Sen's slope estimation method. Compared to linear regression the Sen's slope estimator is not as sensitive to data outliers. In this method, the slope is estimated as the median value of all the slopes that were determined between all possible pairs of data points.

The methods presented above did not take into account the seasonality of data. The seasonal MK test applies the normal MK test separately for each season, which could be, for example, months, quarters of the year, or hours of day, depending on the purpose of use. In the seasonal MK test, the S and VAR(S) are determined separately for each season. The retrieved S and VAR(S) are then summed up, and the Z is calculated in a similar manner to Eqs. 20

and 21 but now using the sums of S and VAR(S) that were calculated separately for each season. Forming the hypotheses and rejecting them is done like for the normal MK test. The seasonal Sen's slope estimator is almost similar to the traditional Sen's slope estimator, but this time the slope between all the data pairs are determined separately for each season. Then, the estimated slope is the median value of all of the slopes regardless of their season.

Due to the strong annual variation in the aerosol data, in this thesis, the seasonal MK test and Sen's slope estimator were applied. The seasons were chosen to be represented by monthly median values of each parameter. The monthly median values smooth out the extreme outliers of hourly measurements and the trend analysis is less affected by outliers or possible erroneous measurements. Similar methods have also been used in several recent articles that presented trends in aerosol measurements (Collaud Coen et al., 2007; Collaud Coen et al., 2013; Li et al., 2014; Zhao et al., 2017).

3.3.2 Iteration of the complex refractive index

As stated in Sect. 2.1, with a known m, the σ_{sca} and σ_{abs} can be derived from size distribution measurements by assuming the particles are spherical and applying the Mie-theory. However, if the σ_{sca}, σ_{abs}, and size distribution are known, the Mie-theory can be applied to derive the m. For example, Virkkula et al. (2011) derived the m by an iterative manner. In this method, the σ_{sca} and σ_{abs} were first modelled by assuming an initial value for the m and by applying the Eq. 3 and the measured size distribution. The modelled σ_{sca} and σ_{abs} were then compared to their measured equivalents, if they did not match within 1 %, the m was varied. The m was iterated in three phases: first, only the real part (n) was varied until the modelled and measured σ_{sca} matched; then, the complex part (k) was varied until the modelled and measured σ_{abs} matched; lastly the n was varied again since the changing k had an effect on the n (and vice versa). To calculate the Mie-scattering and –absorption, we used the MATLAB-scripts by Mätzler (2002).

3.3.3 Estimation of the primary particle fraction

Rodríguez and Cuevas (2007) suggested a method to estimate the fraction of primary particles from the total aerosol number concentration (N) depending on the *eBC* concentration. The method is based on the high correlation between the *eBC* concentration and primary traffic-related particle number concentration (N_P). The method estimates the N_P from the *eBC* concentration by applying a semi-empirical scaling factor S_p

$$N_P = S_P \cdot eBC. \tag{22}$$

The S_P is derived from the observations of the *eBC* and N so that the S_P is the slope of the line that follows the lowest alignment in a N vs. *eBC* concentration plot. In **Paper V**, the S_P was determined as the 0.2, 1, and 5 % values of the N/*eBC*-relation. The estimated number concentration of secondary particles (N_S) is then derived by subtracting the N_P from the N

$$N_S = N - N_P. \tag{23}$$

4 Results and discussion

This chapter presents the main findings of **Papers I–V.** The results are divided in three sections: Sect. 4.1 concentrates on the measurements conducted at SMEAR II studying the relationships between the AOPs, size distribution, chemical composition, and aerosol sources; Sect. 4.2 discusses the spatio-temporal variation in aerosols and presents the observed long-term trends; and lastly Sect. 4.3 discusses the challenges in the absorption measurements.

4.1 Relationships between the AOPs, size distribution, and chemical composition

The long-term comprehensive measurements of the AOPs, aerosol size distribution and NR-PM_1 chemical composition at SMEAR II provided a good basis for the comparison of these parameters. Compared to the size distribution or chemical measurements, the instruments that measure the AOPs are quite common due to their reasonable price and their ease of use. Studying the relations between the AOPs and other parameters for ambient aerosols can help understanding similar behavior in the AOPs at a site that only has optical measurements or that lack either size distribution or chemical composition measurements.

First, Sect. 4.1.1 presents an overview of the AOPs observed at SMEAR II and discusses about the uncertainties of the measurements. Then Sect. 4.1.2 studies the relationships between the AOPs, size distribution, and chemical composition. Section 4.1.3 concludes what the different parameters indicate on the sources of the particles. The long-term measurements at SMEAR II were conducted by TSI 3563, AE-31, DMSP, APS, and ACSM.

4.1.1 Overview on the AOPs at SMEAR II

AOPs at SMEAR II were already studied by Virkkula et al. (2011), who reported the PM_{10} AOPs for a three-year period (2006–2009). **Paper I** repeated the study at SMEAR II, but for a notable longer time series (about 11 and half years), and also presented a shorter period (about seven and half years) of PM_1 AOPs. Statistics of the PM_1 and PM_{10} AOPs at green wavelength (550 nm) are presented in Table 1. Here the values are reported for the period when the PM_1 and PM_{10} measurements were run in parallel (June 2010 – December 2017).

The data of the AOPs at SMEAR II have also been included in two recent studies that combined together AOPs at several stations (Pandolfi et al., 2018; Laj et al., 2020). Compared to those studies, the average values of the extensive AOPs fell in to the expected range between remote and urban stations, as shown by Laj et al. (2020), who joined together data sets of AOPs from tens global GAW stations. According to their analysis, on average, the σ_{sca} and σ_{abs} at SMEAR II were lower than at most of the rural background sites and the σ_{sca} and σ_{abs} were notably higher than at all pristine measurement sites. Compared to other continental sites, the average σ_{sca} and σ_{abs} were rather low (Laj et al., 2020). The comparison of

intensive AOPs showed that SMEAR II, the ω was about 0.9, which was quite low compared to other sites (Laj et al., 2020). This would suggest that the fraction of BC at SMEAR II was a higher than at other similar sites. Pandolfi et al. (2018) combined measurements of σ_{sca} and σ_{bsca} at several European measurement sites and they presented comparisons for α_{sca} and g (derived from b, Eq. 12). The g at SMEAR II was lower compared to other regional and rural sites, which again indicates a relatively higher b. In the comparison of α_{sca}, SMEAR II did not stand out as clearly, but it seemed to be slightly above the average α_{sca} observed at regional and rural sites. Slightly higher α_{sca} and lower g (higher b) would indicate that the size distribution is weighted towards smaller particles than at other sites.

Like shown by Virkkula et al. (2005), the diurnal variations in the AOPs were rather negligible, but the seasonal variations were notable, which was also observed by **Paper I**. Seasonally the differences were the largest between winter and summer, whereas the spring and autumn were more of transition seasons. The causes for the seasonal variations are studied more in the Sect. 4.1.2. The long-term measurements also revealed statistically significant trends for the AOPs, which are presented in Sect. 4.2.3.

Table 1: Median values of the AOPs at SMEAR II (Paper I). The bracketed values are the 25th and 75th percentiles. The values are reported at 550 nm, and the wavelength ranges used in calculating the α_{sca} and α_{abs} were 450 – 700 nm and 370 – 950 nm, respectively. The σabs-related AOPs were determined by using the CC2010 algorithm with Cref = 3.19.

AOP	PM_1	PM_{10}
σ_{sca} (Mm^{-1})	7.1 [3.6, 14.1]	9.6 [5.3, 17.6]
σ_{bsca} (Mm^{-1})	1.1 [0.6, 2.0]	1.4 [0.8, 2.4]
σ_{abs} (Mm^{-1})	1.1 [0.6, 2.0]	1.2 [0.7, 2.2]
ω	0.87 [0.81, 0.91]	0.89 [0.85, 0.92]
b	0.15 [0.13, 0.17]	0.14 [0.13, 0.16]
α_{sca}	2.41 [2.09, 2.66]	1.92 [1.57, 2.12]
α_{abs}	1.03 [0.80, 1.19]	0.97 [0.76, 1.11]
n	1.487 [1.456, 1.516]	1.525 [1.495, 1.550]
k	0.021 [0.014, 0.031]	0.014 [0.009, 0.023]
RFE ($W\ m^{-2}$)	-	-24 [-27, -20]

4.1.1.1 Uncertainties in the σ_{abs} measurements at SMEAR II

As stated in Sect. 3.1, there are large uncertainties related to the σ_{abs} measurements. The effect of different AE-31 algorithms on the observed AOPs at SMEAR II were studied in detail in **Paper II**, which gives more insight on the uncertainties of the reported AOPs in **Paper I.**

Paper I reported AOPs that were derived from AE-31 measurements by using the algorithm by Collaud Coen et al. (2010) (hereon referred as CC2010). It used $C_{ref} = 3.19$ that was the median value of the relation presented by Eq. 18, where the σ_{ATN}, which was measured by the AE-31 and corrected by CC2010, was compared to the $\sigma_{abs,ref}$ measured by the MAAP. Later, **Paper II** determined the C_{ref} as a fit that resulted to $C_{ref} = 2.99$ for CC2010. This value was about 6 % lower than the one used in **Paper I**. If $C_{ref} = 2.99$ was used in **Paper I**, the resulted σ_{abs}, ω, α_{abs}, and *RFE* are presented in Table 2, which is comparable to the PM_{10} results in Table 1. Even though, the resulted σ_{abs} for using the $C_{ref} = 2.99$ was about 8 % higher than for $C_{ref} = 3.19$, the difference still fits within the 23 % uncertainty of the AE-31 measurements (**Paper I**). For the α_{abs}, ω, and *RFE* values, the differences were even smaller.

The σ_{abs} does not depend on the C_{ref} alone, but also on the correction algorithm used. This was tested by deriving the σ_{abs} according to the recommendations by the GAW, i.e., by setting the $R(ATN)$ to unity and using $C_{ref} = 3.5$ (WMO/GAW, 2016). This method is hereon referred as WMO2016. The results of applying the WMO2016 for the PM_{10} AOPs are also shown in Table 2. Compared to the σ_{abs} given in Table 1, the σ_{abs} derived by using the WMO2016 method, decreased about 8 %, but still fitting within the uncertainty limits of the AE-31. Even the 18 % difference between the median σ_{abs} for the WMO2016- and CC2010-derived data presented in Table 2 fits within the 23 % uncertainty.

Table 2: Median values of the PM_{10} AOPs at SMEAR II. The bracketed values are the 25th and 75th percentiles. The AOPs that were derived by the WMO2016 ($C_{ref} = 3.5$) and CC2010 ($C_{ref} = 2.99$) algorithms. The values are reported at 550 nm, and the wavelength range used to calculate the α_{abs} was 370 – 950 nm. The values were calculated for the same period as the values in Table 1.

AOP PM_{10}	WMO2016 ($C_{ref} = 3.5$)	CC2010 ($C_{ref} = 2.99$)
σ_{abs} (Mm^{-1})	1.1 [0.6, 2.0]	1.3 [0.7, 2.4]
ω	0.90 [0.86, 0.93]	0.88 [0.84, 0.92]
α_{abs}	0.97 [0.82, 1.10]	0.97 [0.76, 1.12]
RFE ($W\ m^{-2}$)	-24 [-27, -20]	-23 [-26, -19]

Paper I studied the sensitivity of the AOPs on the correction algorithm by determining the AOPs for data that was derived by using the algorithm by Arnott et al. (2005) (hereon referred as A2005). The A2005 was applied in a similar manner to Virkkula et al. (2011) who used the C_{ref} and τ values recommended for ambient measurements (Arnott et al., 2005). The results, which are presented in Table S2 in **Paper I**, did not differ at 520 nm, but the mean σ_{abs} derived by A2005 at 370 nm and 950 were about 10 % higher and 17 % lower than the σ_{abs} derived by CC2010. The changes in the wavelength dependency increased the average α_{abs} drastically; the mean α_{abs} derived by A2005 (in the 370 – 950 nm range) was about 43 % higher than that derived by CC2010. This was significantly over the 28 % uncertainty that derived for the α_{abs} (Table S3 in **Paper I**).

To conclude, deriving the σ_{abs} from AE-31 measurements by applying different correction algorithms and suggested C_{ref} values did not yield remarkably different σ_{abs} or its derivatives (ω and *RFE*) if the high uncertainty of the AE-31 measurements was considered. At least this was the case at 550 nm. The effect of different algorithms on the σ_{abs} wavelength dependency were significant, which was discussed in **Paper II**. According to **Paper II**, the α_{abs} determined from CC2010 data actually resulted to the lowest average α_{abs} of the different correction algorithms tested for the AE-31, and on the contrary, the α_{abs} derived from A2005 resulted to the highest averages.

4.1.2 Variations in the AOPs, size distribution and chemical composition

The AOPs, size distribution and chemical composition all had distinctive annual cycles (**Papers I** and **III**). As expected, the seasonal variations in the extensive AOPs followed closely the seasonal variation of the different particle mass concentration parameters (*NR-PM*$_1$, *PM*$_{2.5}$; **Papers I** and **III**). The seasonal variations in the σ_{sca}, σ_{bsca}, *NR-PM*$_1$, and *PM*$_{2.5}$ were bimodal: two local maxima occurred around February and July; and two local minima occurred around April and October. The σ_{abs} had a maximum also in February, but the seasonal variation in the σ_{abs} differed from the other extensive parameters so that it was monomodal and the σ_{abs} reached its minimum in June.

Paper I studied the relationships between the PM_1 and PM_{10} AOPs and size distribution. The study showed that the size dependent b and α_{sca} increased in summer and decreased in winter for both PM_{10} and PM_1 measurements. A closer look in the size distribution data showed that the variation was mainly due to shifts in the accumulation mode, which moved towards larger sizes in winter and smaller sizes in summer. Even though the coarse mode was significantly smaller in winter than during other seasons (i.e., higher fraction of PM_1), either the PM_{10} b or α_{sca} were not affected. This would indicate that by measuring only the AOPs of PM_{10}, it would be difficult to make conclusions on the coarse mode particles. However, if also the PM_1 AOPs are measured, the differences between the PM_1 and PM_{10} measurements gives more information especially on the scattering properties of the coarse mode.

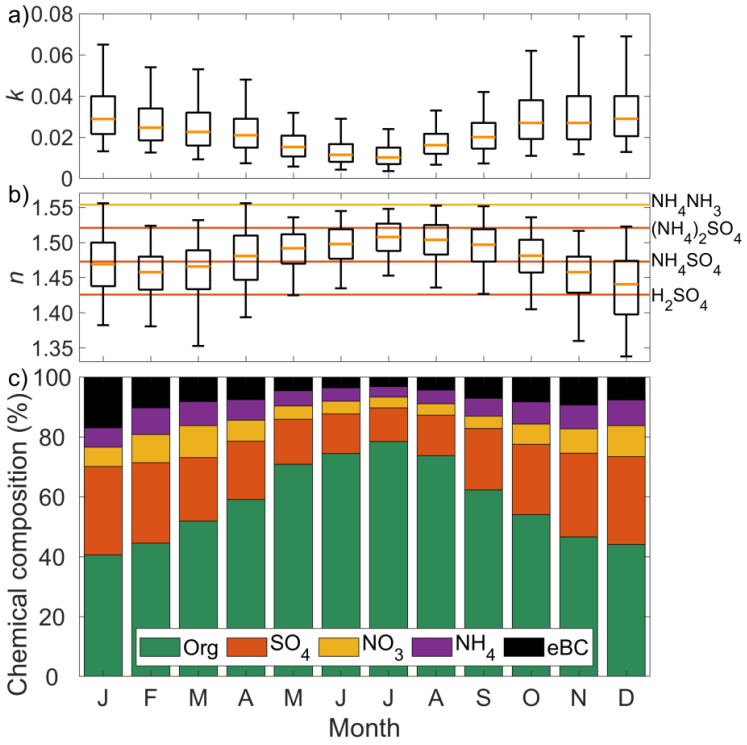

Figure 4: Seasonal variation in the complex refractive index components a) *k*, b) *n*, and c) chemical composition of PM_1 at SMEAR II. In b) also the *n* values of H_2SO_4, NH_4HSO_4, NH_4NH_3 and $(NH_4)_2SO_4$ are plotted in the figure as an example. The data of the chemical composition was presented in Paper III and the data of the *n* and *k* in Paper I.

The sensitivity ranges of the α_{sca} and *b* for multimodal size distributions are rather complex (Schuster et al., 2006; Virkkula et al., 2011). According to Collaud Coen et al. (2007) the *b* is sensitive to particles smaller than 400 nm in diameter and the sensitivity of the α_{sca} is the highest for the size range of 500 – 800 nm. In fact, **Paper I** showed that in winter, especially the concentration of particles in the size range 500 – 800 nm increased compared to other seasons. This could explain why the α_{sca} did not show any increase in winter when the coarse mode was at its minimum concentration.

The analysis of the NR-PM_1 chemical composition gave insight on the scattering fraction of the particles as the absorbing fraction is assumed to be mainly caused by BC. An overview of the seasonal variations in the chemical components (*NR-PM*$_1$ and *eBC*) is presented in Fig. 4c. In general, the organic species were the main component of the NR-PM_1 all year round and their fraction and absolute amount was the highest in summer, which explained the summer peak of σ_{sca} (**Paper III**). Sulfates were the second largest and nitrates the third largest factor. The fraction and absolute amount of the inorganic species (sulfates and nitrates) increased in winter. The winter peak of the σ_{sca} was mainly due to this increase but also due to a slight absolute increase in the organic species (**Paper III**).

Figures 4a and b present the iterated real and imaginary parts of the *m* (see Sect. 3.3.2) for the PM_1. Both the *k* and *n* had unimodal seasonal variations, but their maximum and minimum values occurred inversely. The *n* had its minimum in winter and maximum in summer, for the *k* the situation was the opposite. To give a standpoint on how the chemical composition affects the *m*, Fig. 4b shows the *n* of sulfuric acid, ammonium bisulfate, and ammonium sulfate (H_2SO_4, n = 1.426; NH_4HSO_4, n = 1.473; $(NH_4)_2HSO_4$, n = 1.521; Seinfeld & Pandis, 2016) as well as that of ammonium nitrate (NH_4NO_3, n = 1.554; Tang, 1996), of which especially ammonium sulfate and ammonium nitrate are abundant in the atmosphere. The *n* of organic aerosol (OA) could not be marked in Fig. 4b since the *n* varies notably between different species and measurement techniques (Moise et al., 2015).

On average, the iterated *n* for the ambient aerosol stays below the *n* for ammonium sulfate and ammonium nitrate for the whole year. On average, the *n* is closest to that of ammonium bisulfate and in December the median *n* is actually close to the *n* of sulfuric acid. Due to the high fraction of OA, which has unknown *n*, it is complicated to estimate the effect of inorganic species to the *n*. Also due to the fact that in deriving the *m* the PM is assumes homogeneous (Sect. 3.3.2), a probable reason for the annual variation in the *n* is actually the variation in the measured σ_{abs} and ω: in winter the absorbing fraction was relatively higher and the scattering fraction was relatively lower. In summer, when the amount of BC (or other absorbing material decreases), the *n* of ambient aerosols increased towards the *n* of ammonium sulfate, ammonium nitrate, and probably also towards the *n* of OA.

The variation in the *k* was easier to interpret since it followed closely the seasonal variation in *eBC* concentration. Even though it is justified to assume that BC is the main absorbing substance, it must be kept in mind that the σ_{abs} measurements (i.e., *eBC* measurements) can be influenced by several factors, which affect the seasonal variation in σ_{abs} and here the seasonal variations in *k* as well. For example, **Paper II** observed that the C_{ref} at SMEAR II varied seasonally so that it reached its maximum in summer and minimum in winter. Since the σ_{abs} data were retrieved by using a constant C_{ref}, considering the annual variation in C_{ref} would amplify the seasonal variation in the σ_{abs} and *k*. The σ_{abs} can also be increased by the more pronounced lensing effect in summer, which was considered in **Paper I**.

4.1.3 Conclusions on the sources of aerosol particles

Paper I suggested that in winter, the anthropogenic influence was clearly higher compared to the summer according to the seasonal variations in the σ_{abs} (or *eBC*), ω, b, and α_{scat}. According to the intensive properties, in winter, the fraction of BC was high (low ω) and the particle size distribution consisted of larger particles since the accumulation mode had shifted towards larger particles (low *b* and α_{scat}), which could have been due to greater fraction of long-range transport pollution and more aged particles than in summer. The seasonal variation in the NR-PM1 chemical composition supported this claim since **Paper III** reported elevated concentrations of sulfate and nitrate aerosols and their pre-cursor gases (SO_2 and NO_x) in winter. These markers are related to fossil fuel combustion.

However, the sulfates and nitrates are not tracers for biomass burning, which in southern Finland is a significant contribution to local particulate emissions especially during the cold period due to domestic wood combustion (Karvosenoja et al., 2011). The elevated *eBC* levels in winter were partly explained by the regional wood combustion emissions. One marker for the wood combustion is the ACSM f_{60}-signal, which indicates levoglucosan-species that are formed in cellulose pyrolysis (Alfarra et al., 2007). **Paper III** reported higher f_{60}-signal in winter, which supports the assumption of observed wood combustion aerosol at SMEAR II.

Since the σ_{abs} measurements were conducted at multiple wavelengths, using a BC source apportionment model, which estimates the fraction of BC from traffic and wood combustion, was possible (Sandradewi et al., 2008; Zotter et al., 2017). The model applies the α_{abs} so that purely traffic-related BC is indicated by α_{abs} value of unity and purely wood-combustion related BC is indicated by α_{abs} = 1.6. The observed relative variation in the α_{abs} indicated that the fraction of BC from wood combustion increased towards the cold period as the α_{abs} is the highest in winter and lowest in summer (**Paper I**). However, applying the source apportionment model at SMEAR II was challenging since the seasonal variation in the α_{abs} showed that about a third of the time the α_{abs} was below unity, which would yield an unphysical fraction (> 100 %) of BC from traffic (**Paper I**). The α_{abs} values below unity could be explained by the morphology and the coating of the particles (Liu et al., 2018); for example, heavy coating on relatively large BC cores results to $\alpha_{abs} < 1$ (Lack & Cappa, 2010). The empiric source apportionment model was determined for fairly freshly emitted BC (Sandradewi et al., 2008; Zotter et al., 2017). Therefore, the model might not perform as well at SMEAR II where there are no local sources and the BC is therefore more aged. Also, the use of different correction algorithms has a very large impact on the α_{abs} values as already mentioned in Sect. 4.1.1.1 and discussed more in Sect. 4.3.

For summer, **Paper I** concluded that the AOPs were affected by SOA, since the σ_{sca} increased, the σ_{abs} decreased, and the ω, *b,* and α_{scat} reached their maxima. These factors indicated low contribution of anthropogenic BC and that the accumulation mode shifted towards smaller diameters. Shifting accumulation mode towards smaller sizes could be a result of SOA formation and growth of smaller particles. Also, **Paper III** concluded that the concentration of OA in summer increased due to biogenic SOA since also the monoterpene mixing ratio, which indicates the activity of the forest vegetation, increased.

As shown before, the measurements of the AOPs at visible wavelengths and NR-PM_1 are sensitive to particles that belong in the accumulation and coarse mode (i.e., are mainly larger than ~100 nm). Since the AOPs and NR-PM_1 depend on the volume (or mass) distribution of particles, they do not provide much information of the aerosol number concentration (*N*), which is dominated mainly by particles smaller than 100 nm. The *N* was examined in more detail in **Paper V** that studied the fraction on primary particles by using the *eBC* concentration as an indicator on the primary particle number concentration according to Eqs. 22 and 23. The study estimated that at SMEAR II only about 5 – 16 %, depending on the method used, of the Aitken mode particles were primary in origin. In the accumulation mode, the estimated fraction of primary particles was a bit higher, about 11 – 34 %. For the total *N*,

the fraction of primary particles was about 7 – 21 %. The main result of **Paper V** was that overall a majority of the particles observed at SMEAR II were secondary of origin.

The study did not consider the seasonal variation in the primary or secondary particle fractions in detail. However, according to the method used in **Paper V**, it is evident that the *N* of secondary particles in summer was higher than in winter based on the lower *eBC* concentration in summer (**Paper IV**) and on the fact that the *N* peaks in summer and is lowest in winter (Dal Maso et al., 2008). In winter, the fraction of secondary particles from biogenic sources decrease due to the low temperatures and low VOC emissions from vegetation. However, the secondary particles are also originating from anthropogenic sources, which instead have a greater impact in winter due to increased energy production.

4.2 Spatio-temporal variation in the aerosol particles

Sect. 4.1 already touched the temporal variation in AOPs, size distribution, and chemical composition at one location, SMEAR II. This section broadens the view to consider also the spatial variation of ambient aerosols. The articles included in this study did not include measurements of AOPs at various sites and therefore it is not possible to directly study the spatial variations in the AOPs. However, the articles treated a wide-ranging datasets of eBC and $PM_{2.5}$ concentrations that extended the analysis of aerosols from a boreal forest environment to urban traffic environment and even to a polluted megacity.

4.2.1 Spatial variation

The median *eBC* concentrations in a boreal forest site, urban locations in the HMA, and in a megacity are presented in Table 3. The data collected in the HMA was combined according to station type: the UB sites (UB1–2); the DH sites (DH1–5); and the two TR site groups, which were TR1–4 and TR5–6. Figure 2 in **Paper IV** shows that the grouping of the sites in the HMA worked well for the UB, DH, and TR5–6 sites since the average *eBC* concentration was rather constant in these environments. However, for the TR1–4 there was more variation station by station.

Table 3: Median eBC concentrations at different sites. The bracketed values are the 25th and 75th percentiles. Here the data from some of the stations were combined.

Location	Station	Station type	*eBC* (μg m^{-3})
Boreal forest	SMEAR II	Rural background	0.18 [0.09, 0.35]
HMA	RB1	Regional background	0.19 [0.09, 0.36]
	UB1–2	Urban background	0.38 [0.21, 0.65]
	DH1–5	Detached housing	0.42 [0.23, 0.79]
	TR1–4	Traffic	0.77 [0.41, 1.43]
	TR5–6	Traffic	0.57 [0.32, 0.97]
Megacity	SORPES	Urban background	2.23 [1.34, 4.02]

The results showed that the *eBC* concentration depended clearly on the proximity of the anthropogenic sources. For the sites that located in southern Finland (i.e., all the other sites than SORPES), the *eBC* concentration depended mainly on the station type as expected. The lowest concentrations were measured at the background sites, higher concentrations were observed at UB and DH sites, and the highest at the TR sites (**Paper IV**). The median *eBC* concentration at SORPES, an urban background site in a megacity, was even higher than the 75th percentile at the TR sites in the HMA (**Paper V**). Simply put, even the background levels of air pollution in a Chinese inland megacity were notably higher than the pollution levels in a traffic environment in a seaside city in Southern Finland. In the HMA, the effect of the most prominent BC sources, which were traffic and residential wood combustion (Helin et al., 2018), were seen in the data. It was surprising that the median concentrations of *eBC* at the UB sites were actually lower than at the DH sites. Even though the UB sites were closer to busy traffic lines (but not in proximity), the wood combustion at the DH sites seemed to decrease the air quality more than nearby traffic sources at the UB sites.

In addition to the *eBC* concentration, **Paper IV** analyzed also the $PM_{2.5}$ data. Since *eBC* data originates from σ_{abs}, and the σ_{sca} and $PM_{2.5}$ concentration typically correlate well, it can be assumed that the *eBC* and $PM_{2.5}$ concentration give some insight on the ω. **Paper IV** showed that the $eBC/PM_{2.5}$ ratio was the highest at the TR sites, somewhat lower at the DH sites, and the lowest at the RB sites. It can be concluded that probably the ω was the lowest at the TR sites and highest at the RB sites. This would indicate that the increased amount of *eBC* decreases the ω at more polluted sites. However, high ω does not necessarily indicate better air quality. For example, at the more polluted SORPES, a rather high median value of 0.94 was observed for the ω (Shen et al., 2018).

4.2.2 Seasonal and diurnal variation

Paper IV studied the diurnal and seasonal variation in *eBC* concentrations at different environments ranging from the rural background site SMEAR II to urban traffic sites in the HMA. The results are presented in Fig. 5, which shows well how the dependency of the *eBC* concentration on the meteorological conditions and local anthropogenic sources varied between different environments.

The local anthropogenic emissions governed the seasonal and diurnal variation in the *eBC* concentration at the TR and DH sites. At TR1–4, which were completely dominated by traffic, the seasonal variation was negligible and the *eBC* concentrations followed the traffic rates. At the DH sites, the domestic wood combustion played an important role by increasing the *eBC* concentrations in the evenings and especially during the cold period and in the evenings. At TR5–6, the temporal variation was a combination of those of TR1–4 and DH sites. Since the TR5–6 were located closer to the DH areas than other TR sites (Fig. 3).

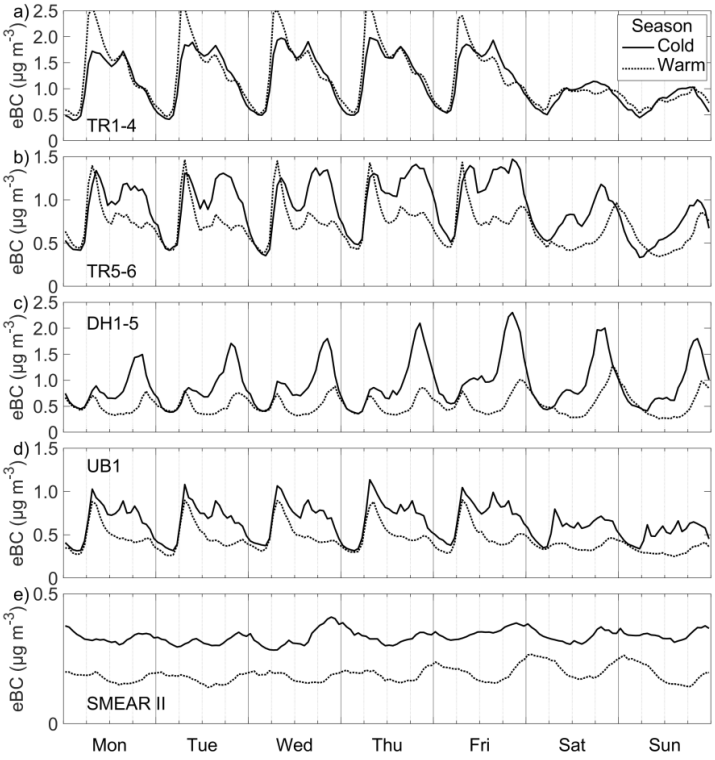

Figure 5: Diurnal variation in the eBC concentration at a) TR1–4, b) TR5–6, c) DH1–5, d) UB1, and e) SMEAR II. The variations are presented separately for each weekday for both the cold (November – March) and warm (May – September) seasons. Data used in the figure is from Paper IV.

The effect of meteorology became more important when the *eBC* concentrations were observed at the background sites with less or no local sources. At UB1, the effect of traffic was clearly visible, but the dilution during the warm season notably decreased the daytime concentrations. At SMEAR II, the meteorology governed the variation in the *eBC* concentration. In summer, the dilution caused by the summertime boundary layer development induced a diurnal cycle so that the *eBC* concentration decreased during the day and increased during the night. In winter, the diurnal variation was more noisy and not as clear as in summer, due to smaller changes in boundary layer height. In general, the *eBC* concentration was generally higher in winter due to shallower boundary layer (i.e., accumulation of pollutants) and long-range transported pollution (**Paper I**).

Paper V researched the diurnal variation in particles at SMEAR II and SORPES, but from the viewpoint of their number concentration. It studied the number concentration of primary and secondary particles in different size modes. In general, **Paper V** showed that at both of the sites at all the times, a majority of the particles were secondary of origin. The highest fraction of primary particles were observed in the accumulation mode during the morning and afternoon rush hour peaks at SORPES supporting the importance of traffic emissions in

reducing air quality. **Paper V** also showed that even though at SMEAR II there were no local anthropogenic sources nearby, forest surrounding the station was an important source for nucleation mode particles. The method was originally developed in urban environment close to traffic emissions, where the *eBC* concentration and *N* generally correlate well. In **Paper V**, however, here the method was applied to background sites where the correlation between the *eBC* and *N* was not as clear.

4.2.3 Long-term trends

The long-term trends were studied for the AOP data from SMEAR II (**Paper I**) and for the air quality data collected at SMEAR II and several sites in the HMA (**Paper IV**). Here the trends from all these different types of sites, ranging from a rural background site to a curbside traffic site are combined. The significance and magnitude of the trends were determined by using the seasonal Mann-Kendall test and Sen's slope estimator (Sect. 3.3.1). A statistical significance level of $s < 0.05$ was required. Table 4 reports the statistically significant trends in extensive properties observed in **Papers I** and **IV** and Fig. 6 presents their time series. Long-term trends were observed at SMEAR II, at one urban background site (UB1), and at three traffic sites (TR1–3). Generally, the trends in urban environment follow the changes in the local emissions, whereas the trends in background sites depend on the changes in the regional emissions and long-transport pollution.

Table 4: The relative trends in the extensive AOPs, as well as in the *eBC* and $PM_{2.5}$ concentrations at various sites. The years included in the trend analysis are also reported. The trends fort the extensive AOPs at SMEAR II are reported for the PM_{10} measurements.

Station	Parameter	Trend (% yr^{-1})	Reported in	Years
SMEAR II	σ_{sca} (PM_{10})	-3.3	Paper I	2006 – 2017
	σ_{bsca} (PM_{10})	-3.2	Paper I	2006 – 2017
	σ_{abs} (PM_{10})	-5.8	Paper I	2006 – 2017
	eBC	-6.3	Paper IV	2006 – 2018
	$PM_{2.5}$	-2.6	Paper IV	2006 – 2018
UB1	*eBC*	-5.7	Paper IV	2012 – 2018
	$PM_{2.5}$	-3.9	Paper IV	2012 – 2018
TR1	*eBC*	-6.5	Paper IV	2011 – 2018
	$PM_{2.5}$	-3.7	Paper IV	2011 – 2018
TR2	*eBC*	-10.6	Paper IV	2012 – 2018
TR3	*eBC*	-12.2	Paper IV	2010, 2015
	$PM_{2.5}$	-5.6	Paper IV	2010, 2015

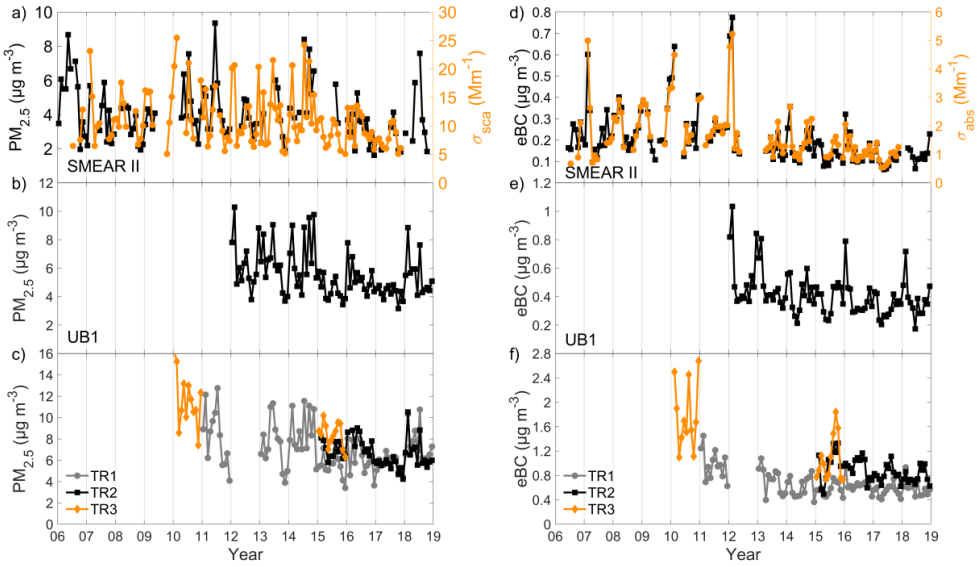

Figure 6: The time series of a) $PM_{2.5}$ and σ_{sca} at SMEAR II, b) $PM_{2.5}$ at UB1, and c) $PM_{2.5}$ at TR1, TR2, and TR3, and d) *eBC* and σ_{abs} at SMEAR II, e) *eBC* at UB1, and f) *eBC* at TR1, TR2, and TR3. The time series of the AOPs were preseted in Paper I, and the time series of the *eBC* and $PM_{2.5}$ concentrations were presented in Paper IV.

At all the sites, which reported statistically significant trends in both $PM_{2.5}$ and *eBC* (SMEAR II, UB1, TR1, and TR3), the *eBC* concentration decreased at a faster rate than the $PM_{2.5}$ concentration, which indicated that especially the PM originating from combustion has decreased. **Paper IV** conducted the trend analysis for the NO_x concentration as well and observed that the NO_x concentration decreased at a rather similar relative rate as the *eBC* concentration. Since NO_x is mainly emitted from traffic, the results suggested that the decreased PM, especially in urban environment, was due to decreased traffic emissions. The *eBC* and NO_x concentrations decreased relatively the fastest during the morning rush hour peak, supporting the assumption of decreased traffic emissions (**Paper IV**).

Part of the decrease in the *eBC* concentration could have been due to changes in wood combustion emissions. However, Anttila (2020) reported no widespread decrease in Finland for the PAH (polycyclic aromatic hydrocarbons) concentrations that would indicate a decrease in biomass burning (Shen et al., 2013). Since the biomass burning has not been regulated in a similar manner as traffic, energy, or industrial emissions (e.g., EU, 2008), it is no surprise that biomass burning emissions did not show a decreasing trend (Anttila, 2020). The residential wood combustion has notable contribution to the regional PM concentration (Savolahti et al., 2016; Vicente & Alves, 2018; Cincinelli et al., 2019), especially in Finland and other Nordic countries (Savolahti et al., 2016; Kukkonen et al., 2020). Due to the adverse health effects of wood combustion emissions (Hime et al., 2018; Daellenbach et al., 2020), policies or regulations considering the biomass burning should also be recalled (Cincinelli et al., 2019).

The amount of PM did not only decrease due to the changes in traffic emissions but also due to a more general decrease in the background concentrations as observed at SMEAR II. **Paper I** reported that in addition to the decrease in the aerosol amount, also an increasing trend in the ω and b were observed, which indicated that the particles were more efficient scatterers and smaller in size than before. A closer study revealed that especially the number of particles in the larger side of the accumulation mode had decreased, which would indicate that on average SMEAR II was influenced less by aged and grown particles, i.e., long-range transported PM. This suggests that especially long-range transported pollution has decreased at SMEAR II.

Several recent long-term trend studies on the AOPs and *eBC* concentration at different environments reported similar observations elsewhere than in Finland (Collaud Coen et al., 2013; Li et al., 2014; Lihavainen et al., 2015; Sherman et al., 2015; Font & Fuller, 2016; Krecl et al., 2017; Kutzner et al., 2018; Pandolfi et al., 2018; Singh et al., 2018; Collaud Coen et al., 2020; Laj et al., 2020; Sun et al., 2020). These studies have observed decreasing trends in the extensive AOPs and *eBC* concentration at various environments. In the urban areas, the decreases in the *eBC* concentration were also connected to traffic emission regulations (Font & Fuller, 2016; Krecl et al., 2017; Kutzner et al., 2018; Singh et al., 2018). The trends observed for the intensive AOPs varied more but at a majority of the sites, the ω and b increased (Collaud Coen et al., 2020; Laj et al., 2020).

From the viewpoint of air quality in general, decrease in the traffic emissions is good news since especially the emissions from traffic are considered to be harmful to health (Krzyżanowski et al., 2005). The observed trends showed that the air quality did not improve only in urban traffic environments, but also in the rural areas. Even though the PM concentrations in the Finnish countryside do not come close to the air quality limits, decreasing the PM also in the areas with low concentrations has a positive effect on the population health (Fischer et al., 2015; Di et al., 2017; Christidis et al., 2019).

To make conclusions how the direct effect of PM on the climate evolved, we need to study the trends in the AOPs. **Paper I** reported increasing trend for the ω as well as for the size dependent b, which indicated that the particles absorbed relatively less light and scattered relatively more light to the backward direction than before. The combined effect of the positive trends in the ω and b lead to a decrease in the *RFE* (see Eq. 13; **Paper I**), which means that the particles observed at SMEAR II cooled the climate more efficiently than before.

If the $PM_{2.5}$ concentration is assumed to represent the scattering fraction of particles, the relatively faster decrease in the *eBC* concentration observed at various sites (**Paper IV**) would suggest that the absorbing fraction of PM decreased relatively faster than the scattering fraction (i.e., the ω increased) also at the HMA sites. According to the parallel measurements of the $PM_{2.5}$ and σ_{sca} at SMEAR II, assuming a correlation between the $PM_{2.5}$ and σ_{sca} seems valid since the monthly median values of these parameters showed a good agreement (Fig. 6a); the *eBC* obviously represents the absorption, as it was derived from the σ_{abs}. It is not possible to draw conclusions on the size dependent parameter b in the HMA based on the $PM_{2.5}$ and *eBC* measurements. However, according to **Paper I**, the *RFE* is more sensitive

to changes in the ω than in the b. Therefore, it is likely, that the *RFE* did not decrease only at the rural SMEAR II, but also in urban environments in the HMA.

In order to mitigate climate warming and to improve air quality, decreasing the anthropogenic greenhouse gas and BC emissions also reduce the emissions of the co-emitted PM and pre-cursor gases that have a cooling effect on the climate (e.g., sulfates). Therefore, even if the PM cools the climate more *efficiently*, the reduction in the total amount of aerosol can actually decrease the *RF* related to the direct effect of aerosols on climate (Baker et al., 2015).

It must be noted that especially in **Paper IV,** the lengths of the data sets at the urban sites were rather short. In aerosol studies, long-term trend analysis should be conducted preferably for at least ten-year-long time series (e.g., Collaud Coen et al., 2020) since also the year-to-year variability due to meteorological conditions may induce a trend in aerosol concentrations. However, also shorter time series can yield realistic trends if the signal is strong enough and the changes in meteorological conditions are considered. For example, efficient renewal of the local bus fleet or banning a street from private vehicles can be seen in the local air quality data almost immediately (Titos et al., 2015), whereas observing a decreasing signal in a background site needs much longer period of measurements. Since the shorter time series can show a rapid change in the pollutant concentrations, they should not be automatically excluded from the trend analysis.

4.3 Effect of algorithms on the filter-based absorption measurements

Paper II utilized the comprehensive σ_{abs} measurements that were conducted for ambient data at SMEAR II during 2013 –2015 simultaneously with AE-31, PSAP, and MAAP. In addition to the instrument comparison, **Paper II** also compared the various correction algorithms, which are used to retrieve the σ_{abs} from the PSAP and AE-31 measurements. Comparison between the MAAP, which was used as the reference instrument, and AE-31 measurements yielded suggestions for the C_{ref} values that are suitable for a boreal forest environment.

The motivation to determine the C_{ref} values at SMEAR II was that the C_{ref} has been observed to vary between different sites (Collaud Coen et al., 2010; Backman et al., 2017), **Paper II** suggested new C_{ref} values that could be used in a boreal forest environment for deriving the σ_{abs} from AE-31 measurements. The resulted C_{ref} values for wavelength 637 nm were 3.00, 3.13, 3.14, and 2.99 for the algorithms suggested by Weingartner et al. (2003), Arnott et al. (2005), Virkkula et al. (2007), and Collaud Coen et al. (2010), respectively. For data that was not corrected for filter loading error, the suggested C_{ref} value was 2.77, which is notably lower than 3.5 that was suggested by the GAW for the not-corrected AE-31 data (WMO/GAW, 2016).

The C_{ref} at SMEAR II, however, was not constant since it varied seasonally so that it increased in summer and decreased in winter. **Paper II** discussed that possibly the seasonal variations in the aerosol size or scattering properties could have been one explanation for

the varying C_{ref}. For example, the increasing b would suggest that the particles scatter light more efficiently in different directions (i.e., increase the optical depth), and that the smaller particles could penetrate deeper in the filter material (i.e., deeper in the absorption of the multiply scattered light increases) (Moteki et al., 2010). Increased ω, which would indicate that the embedded particles scatter light more efficiently,, could add up to the multiple scattering by the filter fibers. Another explanation was probably the variation in the instrumental relative humidity (*RH*) that could affect the filter properties or the penetration depth of the particles in the filter, which would further affect the C_{ref} (**Paper II**).

Paper II showed that after applying the newly derived C_{ref} values, the AE-31 and MAAP data agreed well. For hourly averaged data, the slopes of the linear regression were close to unity and the correlation coefficients were high, about 0.98. However, the AE-31 data that was derived with the algorithms suggested by Arnott et al. (2005) and Collaud Coen et al. (2010) slightly underestimated the σ_{abs} since reducing the fraction of the particulate scattering, which these algorithms take into account, was not considered in deriving the C_{ref}. Also, the σ_{abs} derived from PSAP by using the algorithm suggested by Bond et al. (1999) and Ogren (2010) agreed well with the MAAP data and slope of the linear regression was 1.07 and the correlation coefficient 0.99. The PSAP data corrected with algorithm by Virkkula (2010) overestimated the σ_{abs} more and the slope of the linear regression was 1.27, but the correlation coefficient with MAAP was high (0.97).

The most notable difference between the algorithms and instruments was related to the α_{abs}. The lowest α_{abs} values originated from the AE-31 data that were corrected by the algorithm suggested by Collaud Coen et al., (2010) (hereon CC2010) resulting to a median $\alpha_{abs} = 0.93$. The highest values originated from PSAP data that were corrected by the algorithm suggested by Virkkula et al. (2010) (hereon V2010) and it resulted to a median $\alpha_{abs} = 1.54$ (**Paper II**). Results were in line with study by Backman et al. (2014), who observed a high α_{abs} for the V2010-derived PSAP data, and with a study by Saturno et al. (2017), who observed a low α_{abs} for non-corrected and CC2010-derived AE-31 data. According to an algorithm comparison by Saturno et al. (2017), the best agreement of the α_{abs} derived from AE-31 data with a reference instrument was found for data that was not corrected or that was corrected by CC2010.

When reporting the σ_{abs} or *eBC* concentration it is important to describe the used instruments, algorithms, and constants. If the σ_{abs} or its derivatives are applied in a study, it is also a good practice to test the sensitivity of the results to different correction algorithms. This was done, for example, in Sect. 4.1.1.1, where the effects of different algorithms and the C_{ref} values on the σ_{abs} at SMEAR II were studied. Another example is the sensitivity study in **Paper V**, where the fraction of primary particles were determined with the *eBC* data and the effect by using different correction algorithms were tested. The results shown in **Paper IV** underlined the sensitivity of the α_{abs} for different correction algorithms. Therefore, especially studies that apply the α_{abs} data, such as the ones using the BC source apportionment model (Sandradewi et al., 2008), should consider testing the sensitivity of their results by running the data analysis with different correction algorithms.

5 Review of papers and the author's contribution

Paper I gives a comprehensive view on the AOPs observed at SMEAR II over a ten-year-long measurement period. The AOPs had clear seasonal cycles, so that in summer, the aerosol particles were more efficient scatterers and the aerosol population consisted of smaller particles than in winter. Analysis of the long-term trends showed decreasing trends in the σ_{sca}, σ_{bsca}, and σ_{abs}. The trends in the ω, b, α_{sca}, and size distribution revealed that the aerosol particles were absorbing relatively less light than before and that the weight of the size distribution had moved towards smaller particles especially in the accumulation mode. The trends induced a change in the *RFE*, so that the particles were cooling the atmosphere more efficiently. For this paper, I did the majority of the data analysis and writing.

Paper II studies the challenges related to the filter-based σ_{abs} measurements. The study performs a comparison between three absorption photometers (AE-31, PSAP, and MAAP) and several correction algorithms. The study is based on ambient measurements conducted at SMEAR II. The results showed a good correlation between the instruments after determining suitable C_{ref} values for the AE-31. A comparison of the α_{abs} for the different correction algorithms of the PSAP and AE-31 data revealed that the α_{abs} values depended significantly on the algorithms and instruments. For this paper, I performed the majority of the data analysis and writing.

Paper III reports the annual and year-to-year variation in the NR-PM_1 chemical composition at SMEAR II based on seven years of measurements. The study observed highest *NR-PM1* concentrations in winter and summer. The wintertime peak was associated with inorganic species and the summertime peak was mainly due to SOA that originated from biogenic sources. Apart from data analysis, the study utilized *eBC* data in an instrumental correction algorithms. Here, I provided the *eBC* data and contributed in the writing by commenting and editing the manuscript and by writing about the *eBC* measurements.

Paper IV presents the *eBC*, NO_x, and $PM_{2.5}$ concentrations at various environments in southern Finland and especially in the HMA. The study shows how *eBC* concentration varied both spatially and temporally depending on the local anthropogenic activities that were traffic and residential wood combustion. The long-term trends in *eBC*, NO_x, and $PM_{2.5}$ were statistically decreasing and more detailed analysis showed that the decreasing concentrations were most probably due to a decrease in the local traffic emissions. For this article, I performed the majority of the data analysis and writing.

Paper V investigates the fraction of primary and secondary particles in different aerosol size modes by using *eBC* concentration as a tracer for the primary particle number concentration. The study was applied the measurements at two sites, SMEAR II and SORPES, which represented very different environments. The results showed that the majority of the particles in all size modes were secondary in origin. The highest fraction of primary particles were observed at SORPES for accumulation mode, for which about 50 % of the particles were primary according to our analysis. For this paper, I performed the majority of the data analysis and gave comments to the manuscript.

6 Summary, conclusions, and future outlook

This thesis presented results of aerosol optical properties (AOPs) and equivalent black carbon (*eBC*) measurements at various environments. The focus was on the rural boreal forest site, SMEAR II, which was a common factor for all the papers included in the thesis. The thesis also presented observations from several urban measurement sites located in the Helsinki metropolitan area (HMA) and in Nanjing, a megacity in China.

The results showed that at SMEAR II, the PM had a strong bimodal seasonal variation and the extensive AOPs peaked in winter and summer (**Paper I**). While the scattering coefficient (σ_{sca}) peaked both in winter and in summer, the absorption coefficient (σ_{abs}) peaked only in winter. The backscatter fraction (b) and scattering Ångström exponent (α_{sca}) also showed a clear seasonal variability, reaching the lowest values in winter and indicating that the particle size distribution had more weight on the larger particles. Larger particles, and higher σ_{abs} in winter suggested that the particles originated from anthropogenic combustion sources. Again, in summer, high values of σ_{sca}, α_{sca}, and b, but low σ_{abs} values indicated that the particle population consisted of smaller, secondary aerosol particles that were probably biogenic in origin. Analysis of size distribution measurements showed that especially the shifting of accumulation mode had an effect on the AOPs (**Paper I**). Chemical analysis of the non-refractory PM_1 supported the assumptions and showed that tracers of anthropogenic sources dominated in winter and that the amount of secondary organic aerosol increased in summer (**Papers III** and **V**).

The thesis investigated the concentration of optically measured equivalent black carbon (*eBC*), which originates as a by-product of incomplete combustion. The thesis studied the *eBC* concentrations at the rural background site SMEAR II, at several urban sites in the HMA, and at an urban background site in Nanjing. Compared to the rural boreal environment, which was mainly affected by regional and long-range transported pollution, the effects of anthropogenic sources, such as traffic and residential wood combustion, were clearly seen in the urban areas (**Papers IV** and **V**).

Decreasing trends in aerosol concentration were observed in several different types of environments in southern Finland (**Papers I** and **IV**). According to the trend analysis especially the amount of absorbing aerosol (i.e., black carbon, BC) had decreased. Unfortunately, the length of the chemical composition time series at SMEAR II were yet not long enough for a trend analysis, which would have given information about the trends in different scattering components.

The observed decrease in the amount of aerosol at SMEAR II was linked to a decrease in long-range transported pollution (**Paper I**) and the decreases observed in the HMA were connected to changes in local traffic emissions (**Paper IV**). This thesis could not study whether there were changes in the residential wood combustion emissions. However, according to other studies decreases in the wood combustion emissions were not observed as

they have not been regulated like other pollution sources (Anttila, 2020) even though residential wood combustion is the most significant source for BC in Finland (Rautalahti & Kupiainen, 2016).

From the viewpoint of climate, the relatively faster decrease of *eBC* compared to other chemical components had a positive effect on the climate since then the particles scattered light more efficiently. The radiative forcing efficiency of the ambient aerosol particles became more negative, meaning that the particles cooled down the climate more efficiently (**Paper I**). However, the direct effect of aerosols on the radiative forcing may still have decreased, as also the amount of scattering aerosols had decreased.

Apart from the climate effects, the decreasing aerosol concentration also affected the air quality. The study showed that the concentration of *eBC* decreased relatively faster than that of $PM_{2.5}$ suggesting that the improvements in the air quality were especially due to decreased traffic emissions (**Paper IV**). From the viewpoint of air quality, the decreases in the combustion related *eBC* concentrations and traffic emissions were welcoming news since especially the combustion and traffic related particulate matter has adverse health effects. Air quality did not improve at urban areas only, but also in the background sites.

The thesis also discussed about the challenges related to the measurements of the σ_{abs} and *eBC*, which are typically determined by filter based instruments. This study presented suggestions for correction factors, which could be used with different correction algorithms, that could be applicable at a boreal forest environment (**Paper II**). The effect of different instruments and data retrieval algorithms to the AOPs were also studied. The results showed that especially the α_{sca}, which is commonly used in the BC source apportionment, differs notably between the different instruments and correction algorithms (**Paper II**).

For future reference, the measurements of the *eBC* concentration would be further improved by studying of the relationship between the *eBC* and *EC* and deriving a suitable *MAC* value at SMEAR II for a boreal environment. In addition, the relationship between the *eBC* and *EC* would also provide information on the absorption enhancement effect, which is caused by the coating the BC particles and has a warming effect on the climate (Peng et al., 2016; Liu et al., 2017).

Another measurement improvement related to determining the climate effects of aerosols, would be to measure the AOPs in moist air at SMEAR II. Typically, as was also done in this thesis, the measurements of the AOPs are conducted for dried aerosols ($RH < 40$ %; WMO/GAW, 2016), which does not necessarily represent ambient aerosols as the ambient *RH* can be anything between 10 – 100 %. Since the σ_{sca} depends on the *RH* (Zieger et al., 2015), additional measurements of the σ_{sca} *RH* dependency would be valuable for determining the direct effect of aerosols on climate.

Overall, measurements the AOPs are rather straightforward, cheap, and easy to operate since the instruments are robust and do not require much manual labor from the operator. Still the measurements of scattering, backscattering and absorption coefficients, which can be obtained with just two instruments, can provide a good general view on the aerosol properties

and not just on the optical quantities. Good quality AOP data can indicate the source, chemical composition, and size distribution of the particles.

Comprehensive and long-term in-situ measurements of the environment are crucial in order to understand better the complex processes, feedback cycles, and the impact of humans in the Earth system (Kulmala, 2018). Atmospheric aerosols are just one part of the complex system, but still they have an important role in the Earth's climate. Measurements of the aerosol properties and spatio-temporal variation are used to observe, to model, and to predict the changes happening now and in the future. The observations and predictions based on scientific research are needed in order to set policies and regulations that improve the air quality and mitigate global warming.

References

Aalto, P., Hämeri, K., Becker, E., Weber, R., Salm, J., Mäkelä, J. M., Hoell, C., O'Dowd, C. D., Hansson, H.-C., & Väkevä, M. (2001). Physical characterization of aerosol particles during nucleation events. *Tellus B, 53*(4), 344-358. doi:10.3402/tellusb.v53i4.17127

Adachi, K., Chung, S. H., & Buseck, P. R. (2010). Shapes of soot aerosol particles and implications for their effects on climate. *J Geophys Res-Atmos, 115*(D15). doi:10.1029/2009JD012868

Aksoyoglu, S., Ciarelli, G., El-Haddad, I., Baltensperger, U., & Prévôt, A. S. H. (2017). Secondary inorganic aerosols in Europe: sources and the significant influence of biogenic VOC emissions, especially on ammonium nitrate. *Atmos Chem Phys, 17*(12), 7757-7773. doi:10.5194/acp-17-7757-2017

Albrecht, B. A. (1989). Aerosols, Cloud Microphysics, and Fractional Cloudiness. *Science, 245*(4923), 1227-1230. doi:10.1126/science.245.4923.1227

Alfarra, M. R., Prevot, A. S. H., Szidat, S., Sandradewi, J., Weimer, S., Lanz, V. A., Schreiber, D., Mohr, M., & Baltensperger, U. (2007). Identification of the Mass Spectral Signature of Organic Aerosols from Wood Burning Emissions. *Environmental Science & Technology, 41*(16), 5770-5777. doi:10.1021/es062289b

Anderson, T., Covert, D., Marshall, S., Laucks, M., Charlson, R., Waggoner, A., Ogren, J., Caldow, R., Holm, R., Quant, F., Sem, G., Wiedensohler, A., Ahlquist, N., & Bates, T. (1996). Performance characteristics of a high-sensitivity, three-wavelength, total scatter/backscatter nephelometer. *J Atmos Ocean Tech, 13*(5), 967-986.

Anderson, T., & Ogren, J. A. (1998). Determining aerosol radiative properties using the TSI 3563 integrating nephelometer. *Aerosol Sci Technol, 29*(1), 57-69. doi:10.1080/02786829808965551

Andreae, M. O., & Gelencsér, A. (2006). Black carbon or brown carbon? The nature of light-absorbing carbonaceous aerosols. *Atmos Chem Phys, 6*(10), 3131-3148. doi:10.5194/acp-6-3131-2006

Andrews, E., Sheridan, P., Fiebig, M., McComiskey, A., Ogren, J., Arnott, P., Covert, D., Elleman, R., Gasparini, R., Collins, D., Jonsson, H., Schmid, B., & Wang, J. (2006). Comparison of methods for deriving aerosol asymmetry parameter. *J Geophys Res-Atmos, 111*(D5). doi:10.1029/2004JD005734

Anttila, P. (2020). *Air quality trends in Finland, 1994-2018.* (PhD), University of Helsinki, Helsinki. (Finnish Meteorological Institute Contributions No. 163)

Arnott, W. P., Hamasha, K., Moosmüller, H., Sheridan, P. J., & Ogren, J. A. (2005). Towards aerosol light-absorption measurements with a 7-wavelength Aethalometer: Evaluation with a photoacoustic instrument and 3-wavelength nephelometer. *Aerosol Sci Technol, 39*(1), 17-29. doi:10.1080/027868290901972

Asmi, A., Collaud Coen, M., Ogren, J., Andrews, E., Sheridan, P., Jefferson, A., Weingartner, E., Baltensperger, U., Bukowiecki, N., Lihavainen, H., Kivekäs, N., Asmi, E., Aalto, P. P., Kulmala, M., Wiedensohler, A., Birmili, W., Hamed, A., O'Dowd, C., Jennings, S., Weller, R., Flentje, H., Fjaeraa, A. M., Fiebig, M., Myhre, C. L., Hallar, A. G., Swietlicki, E., Kristensson, A., & Laj, P. (2013). Aerosol decadal trends–Part 2: In-situ aerosol particle number concentrations at GAW and ACTRIS stations. *Atmos Chem Phys, 13*(2), 895-916. doi:10.5194/acp-13-895-2013

Backman, J., Schmeisser, L., Virkkula, A., Ogren, J. A., Asmi, E., Starkweather, S., Sharma, S., Eleftheriadis, K., Uttal, T., Jefferson, A., Bergin, M., Makshtas, A., Tunved, P.,

& Fiebig, M. (2017). On Aethalometer measurement uncertainties and an instrument correction factor for the Arctic. *Atmos Meas Tech, 10*(12), 5039-5062. doi:10.5194/amt-10-5039-2017

Backman, J., Virkkula, A., Vakkari, V., Beukes, J., Van Zyl, P., Josipovic, M., Piketh, S., Tiitta, P., Chiloane, K., Petäjä, T., Kulmala, M., & Laakso, L. (2014). Differences in aerosol absorption Ångström exponents between correction algorithms for a particle soot absorption photometer measured on the South African Highveld, Atmos. *Atmos Meas Tech, 7*(12), 4285-4298. doi:10.5194/amt-7-4285-2014

Baker, L. H., Collins, W. J., Olivié, D. J. L., Cherian, R., Hodnebrog, Ø., Myhre, G., & Quaas, J. (2015). Climate responses to anthropogenic emissions of short-lived climate pollutants. *Atmos Chem Phys, 15*(14), 8201-8216. doi:10.5194/acp-15-8201-2015

Beuttell, R., & Brewer, A. (1949). Instruments for the measurement of the visual range. *J Sci Instrum, 26*(11), 357-359.

Bond, T. C., Anderson, T. L., & Campbell, D. (1999). Calibration and intercomparison of filter-based measurements of visible light absorption by aerosols. *Aerosol Sci Technol, 30*(6), 582-600. doi:10.1080/027868299304435

Bond, T. C., Covert, D. S., & Müller, T. (2009). Truncation and angular-scattering corrections for absorbing aerosol in the TSI 3563 nephelometer. *Aerosol Sci Technol, 43*(9), 866-871. doi:10.1080/02786820902998373

Bond, T. C., Doherty, S. J., Fahey, D. W., Forster, P. M., Berntsen, T., DeAngelo, B. J., Flanner, M. G., Ghan, S., Kärcher, B., Koch, D., Kinne, S., Kondo, Y., Quinn, P. K., Sarofim, M. C., Schultz, M. G., Schulz, M., Venkataraman, C., Zhang, S., Bellouin, N., Guttikunda, S. K., Hopke, P. K., Jacobson, M. Z., Kaiser, J. W., Klimont, Z., Lohmann, U., Schwartz, J. P., Shindell, D., Storelvmo, T., Warren, S. G., & Zender, C. S. (2013). Bounding the role of black carbon in the climate system: A scientific assessment. *J Geophys Res-Atmos, 118*(11), 5380-5552. doi:10.1002/jgrd.50171

Bond, T. C., Habib, G., & Bergstrom, R. W. (2006). Limitations in the enhancement of visible light absorption due to mixing state. *J Geophys Res-Atmos, 111*(D20). doi:10.1029/2006JD007315

Charlson, R., Horvath, H., & Pueschel, R. F. (1967). The direct measurement of atmospheric light scattering coefficient for studies of visibility and pollution. *Atmospheric Environment (1967), 1*(4), 469-478. doi:10.1016/0004-6981(67)90062-5

Charlson, R., Schwartz, S., Hales, J., Cess, R. D., Coakley, J. J., Hansen, J., & Hofmann, D. (1992). Climate forcing by anthropogenic aerosols. *Science, 255*(5043), 423-430. doi:10.1126/science.255.5043.423

Christidis, T., Erickson, A. C., Pappin, A. J., Crouse, D. L., Pinault, L. L., Weichenthal, S. A., Brook, J. R., van Donkelaar, A., Hystad, P., Martin, R. V., Tjepkema, M., Burnett, R. T., & Brauer, M. (2019). Low concentrations of fine particle air pollution and mortality in the Canadian Community Health Survey cohort. *Environmental Health, 18*(1), 84. doi:10.1186/s12940-019-0518-y

Cincinelli, A., Guerranti, C., Martellini, T., & Scodellini, R. (2019). Residential wood combustion and its impact on urban air quality in Europe. *Current Opinion in Environmental Science & Health, 8*, 10-14. doi:10.1016/j.coesh.2018.12.007

Cohen, A. J., Brauer, M., Burnett, R., Anderson, H. R., Frostad, J., Estep, K., Balakrishnan, K., Brunekreef, B., Dandona, L., Dandona, R., Feigin, V., Freedman, G., Hubbell, B., Jobling, A., Kan, H., Knibbs, L., Liu, Y., Martin, R., Morawska, L., Pope, C. A., Shin, H., Straif, K., Shaddick, G., Thomas, M., van Dingenen, R., van Donkelaar, A., Vos, T., Murray, C. J. L., & Forouzanfar, M. H. (2017). Estimates and 25-year

trends of the global burden of disease attributable to ambient air pollution: an analysis of data from the Global Burden of Diseases Study 2015. *The Lancet, 389*(10082), 1907-1918. doi:10.1016/S0140-6736(17)30505-6

Collaud Coen, M., Andrews, E., Alastuey, A., Arsov, T. P., Backman, J., Brem, B. T., Bukowiecki, N., Couret, C., Eleftheriadis, K., Flentje, H., Fiebig, M., Gysel-Beer, M., Hand, J. L., Hoffer, A., Hooda, R., Hueglin, C., Joubert, W., Keywood, M., Kim, J. E., Kim, S. W., Labuschagne, C., Lin, N. H., Lin, Y., Lund Myhre, C., Luoma, K., Lyamani, H., Marinoni, A., Mayol-Bracero, O. L., Mihalopoulos, N., Pandolfi, M., Prats, N., Prenni, A. J., Putaud, J. P., Ries, L., Reisen, F., Sellegri, K., Sharma, S., Sheridan, P., Sherman, J. P., Sun, J., Titos, G., Torres, E., Tuch, T., Weller, R., Wiedensohler, A., Zieger, P., & Laj, P. (2020). Multidecadal trend analysis of in situ aerosol radiative properties around the world. *Atmos Chem Phys, 20*(14), 8867-8908. doi:10.5194/acp-20-8867-2020

Collaud Coen, M., Andrews, E., Asmi, A., Baltensperger, U., Bukowiecki, N., Day, D., Fiebig, M., Fjæraa, A. M., Flentje, H., Hyvärinen, A., Jefferson, A., Jennings, S., Kouvarakis, G., Lihavainen, H., Lund Myhre, C., Malm, W., Mihalopoulos, N., Molenar, J., O'Dowd, C., Ogren, J. A., Schichtel, B., Sheridan, P., Virkkula, A., Weingartner, E., Weller, R., & Laj, P. (2013). Aerosol decadal trends–Part 1: In-situ optical measurements at GAW and IMPROVE stations. *Atmos Chem Phys, 13*(2), 869-894. doi:10.5194/acp-13-869-2013

Collaud Coen, M., Weingartner, E., Apituley, A., Ceburnis, D., Fierz-Schmidhauser, R., Flentje, H., Henzing, J., Jennings, S. G., Moerman, M., Petzold, A., Schmid, O., & Baltensperger, U. (2010). Minimizing light absorption measurement artifacts of the Aethalometer: evaluation of five correction algorithms. *Atmos Meas Tech, 3*(2), 457-474. doi:10.5194/amt-3-457-2010

Collaud Coen, M., Weingartner, E., Nyeki, S., Cozic, J., Henning, S., Verheggen, B., Gehrig, R., & Baltensperger, U. (2007). Long-term trend analysis of aerosol variables at the high-alpine site Jungfraujoch. *J Geophys Res-Atmos, 112*(D13). doi:10.1029/2006JD007995

Crosby, P., & Koerber, B. W. (1963). Scattering of light in the lower atmosphere. *J Opt Soc Am, 53*(3), 358-361. doi:10.1364/JOSA.53.000358

Daellenbach, K. R., Uzu, G., Jiang, J., Cassagnes, L.-E., Leni, Z., Vlachou, A., Stefenelli, G., Canonaco, F., Weber, S., Segers, A., Kuenen, J. J. P., Schaap, M., Favez, O., Albinet, A., Aksoyoglu, S., Dommen, J., Baltensperger, U., Geiser, M., El Haddad, I., Jaffrezo, J.-L., & Prévôt, A. S. H. (2020). Sources of particulate-matter air pollution and its oxidative potential in Europe. *Nature, 587*(7834), 414-419. doi:10.1038/s41586-020-2902-8

Dal Maso, M., Hyvärinen, A., Komppula, M., Tunved, P., Kerminen, V.-M., Lihavainen, H., Öviisanen, Y., Hansson, H.-C., & Kulmala, M. (2008). Annual and interannual variation in boreal forest aerosol particle number and volume concentration and their connection to particle formation. *Tellus B: Chemical and Physical Meteorology, 60*(4), 495-508. doi:10.1111/j.1600-0889.2008.00366.x

Delene, D. J., & Ogren, J. A. (2002). Variability of aerosol optical properties at four North American surface monitoring sites. *J Atmos Sci, 59*(6), 1135-1150.

Deshler, T. (2008). A review of global stratospheric aerosol: Measurements, importance, life cycle, and local stratospheric aerosol. *Atmos Res, 90*(2), 223-232. doi:10.1016/j.atmosres.2008.03.016

Di, Q., Wang, Y., Zanobetti, A., Wang, Y., Koutrakis, P., Choirat, C., Dominici, F., & Schwartz, J. D. (2017). Air Pollution and Mortality in the Medicare Population. *New England Journal of Medicine, 376*(26), 2513-2522. doi:10.1056/NEJMoa1702747

Ding, A., Nie, W., Huang, X., Chi, X., Sun, J., Kerminen, V.-M., Xu, Z., Guo, W., Petäjä, T., Yang, X., Kulmala, M., & Fu, C. (2016a). Long-term observation of air pollution-weather/climate interactions at the SORPES station: a review and outlook. *Frontiers of Environmental Science & Engineering, 10*(5), 15. doi:10.1007/s11783-016-0877-3

Ding, A. J., Huang, X., Nie, W., Sun, J. N., Kerminen, V. M., Petäjä, T., Su, H., Cheng, Y. F., Yang, X. Q., Wang, M. H., Chi, X. G., Wang, J. P., Virkkula, A., Guo, W. D., Yuan, J., Wang, S. Y., Zhang, R. J., Wu, Y. F., Song, Y., Zhu, T., Zilitinkevich, S., Kulmala, M., & Fu, C. B. (2016b). Enhanced haze pollution by black carbon in megacities in China. *Geophys Res Lett, 43*(6), 2873-2879. doi:10.1002/2016GL067745

Drinovec, L., Močnik, G., Zotter, P., Prévôt, A., Ruckstuhl, C., Coz, E., Rupakheti, M., Sciare, J., Müller, T., Wiedensohler, A., & Hansen, A. D. A. (2015). The "dual-spot" Aethalometer: an improved measurement of aerosol black carbon with real-time loading compensation. *Atmos Meas Tech, 8*(5), 1965-1979. doi:10.5194/amt-8-1965-2015

Dusek, U., Frank, G. P., Hildebrandt, L., Curtius, J., Schneider, J., Walter, S., Chand, D., Drewnick, F., Hings, S., Jung, D., Borrmann, S., & Andreae, M. O. (2006). Size Matters More Than Chemistry for Cloud-Nucleating Ability of Aerosol Particles. *Science, 312*(5778), 1375-1378. doi:10.1126/science.1125261

Ehn, M., Thornton, J. A., Kleist, E., Sipilä, M., Junninen, H., Pullinen, I., Springer, M., Rubach, F., Tillmann, R., Lee, B., Lopez-Hilfiker, F., Andres, S., Acir, I.-H., Rissanen, M., Jokinen, T., Schobesberger, S., Kangasluoma, J., Kontkanen, J., Nieminen, T., Kurtén, T., Nielsen, L. B., Jørgensen, S., Kjaergaard, H. G., Canagaratna, M., Maso, M. D., Berndt, T., Petäjä, T., Wahner, A., Kerminen, V.-M., Kulmala, M., Worsnop, D. R., Wildt, J., & Mentel, T. F. (2014). A large source of low-volatility secondary organic aerosol. *Nature, 506*(7489), 476-479. doi:10.1038/nature13032

Directive 2008/50/EC of the European Parliament and of the Council of 21 May 2008 on ambient air quality and cleaner air for Europe, (2008).

Fialho, P., Hansen, A. D. A., & Honrath, R. E. (2005). Absorption coefficients by aerosols in remote areas: a new approach to decouple dust and black carbon absorption coefficients using seven-wavelength Aethalometer data. *J Aerosol Sci, 36*(2), 267-282. doi:10.1016/j.jaerosci.2004.09.004

Fischer, P. H., Marra, M., Ameling, C. B., Hoek, G., Beelen, R., de Hoogh, K., Breugelmans, O., Kruize, H., Janssen, N. A. H., & Houthuijs, D. (2015). Air Pollution and Mortality in Seven Million Adults: The Dutch Environmental Longitudinal Study (DUELS). *Environ Health Perspect, 123*(7), 697-704. doi:10.1289/ehp.1408254

Font, A., & Fuller, G. W. (2016). Did policies to abate atmospheric emissions from traffic have a positive effect in London? *Environ Pollut, 218*, 463-474. doi:10.1016/j.envpol.2016.07.026

Gani, S., Bhandari, S., Patel, K., Seraj, S., Soni, P., Arub, Z., Habib, G., Hildebrandt Ruiz, L., & Apte, J. S. (2020). Particle number concentrations and size distribution in a polluted megacity: the Delhi Aerosol Supersite study. *Atmos Chem Phys, 20*(14), 8533-8549. doi:10.5194/acp-20-8533-2020

Gilbert, R. O. (1987). *Statistical methods for environmental pollution monitoring*. New York: John Wiley & Sons.

Hadley, O. L., & Kirchstetter, T. W. (2012). Black-carbon reduction of snow albedo. *Nat Clim Change, 2*(6), 437-440. doi:10.1038/nclimate1433

Hari, P., & Kulmala, M. (2005). Station for measuring ecosystem–atmosphere relations. *Boreal Environ Res, 10*, 315-322.

Haywood, J., & Shine, K. (1995). The effect of anthropogenic sulfate and soot aerosol on the clear sky planetary radiation budget. *Geophys Res Lett, 22*(5), 603-606. doi:10.1029/95GL00075

Helin, A., Niemi, J. V., Virkkula, A., Pirjola, L., Teinilä, K., Backman, J., Aurela, M., Saarikoski, S., Rönkkö, T., Asmi, E., & Timonen, H. (2018). Characteristics and source apportionment of black carbon in the Helsinki metropolitan area, Finland. *Atmos Environ, 190*, 87-98. doi:10.1016/j.atmosenv.2018.07.022

Hellén, H., Kangas, L., Kousa, A., Vestenius, M., Teinilä, K., Karppinen, A., Kukkonen, J., & Niemi, J. V. (2017). Evaluation of the impact of wood combustion on benzo [a] pyrene (BaP) concentrations; ambient measurements and dispersion modeling in Helsinki, Finland. *Atmos Chem Phys, 17*(5), 3475-3487. doi:10.5194/acp-17-3475-2017

Highwood, E. J., & Kinnersley, R. P. (2006). When smoke gets in our eyes: The multiple impacts of atmospheric black carbon on climate, air quality and health. *Environ Int, 32*(4), 560-566. doi:10.1016/j.envint.2005.12.003

Hime, N. J., Marks, G. B., & Cowie, C. T. (2018). A comparison of the health effects of ambient particulate matter air pollution from five emission sources. *International journal of environmental research, 15*(6), 1206. doi:10.3390/ijerph15061206

Hinds, W. C. (1999). *Aerosol technology: properties, behavior, and measurement of airborne particles*: John Wiley & Sons.

Holben, B. N., Tanré, D., Smirnov, A., Eck, T. F., Slutsker, I., Abuhassan, N., Newcomb, W. W., Schafer, J. S., Chatenet, B., Lavenu, F., Kaufman, Y. J., Castle, J. V., Setzer, A., Markham, B., Clark, D., Frouin, R., Halthore, R., Karneli, A., O'Neill, N. T., Pietras, C., Pinker, R. T., Voss, K., & Zibordi, G. (2001). An emerging ground-based aerosol climatology: Aerosol optical depth from AERONET. *J Geophys Res-Atmos, 106*(D11), 12067-12097. doi:10.1029/2001JD900014

Hoppel, W. A., Fitzgerald, J. W., Frick, G. M., Larson, R. E., & Mack, E. J. (1990). Aerosol size distributions and optical properties found in the marine boundary layer over the Atlantic Ocean. *J Geophys Res-Atmos, 95*(D4), 3659-3686. doi:10.1029/JD095iD04p03659

Janssen, N. A. H., Hoek, G., Simic-Lawson, M., Fischer, P., Van Bree, L., Ten Brink, H., Keuken, M., Atkinson, R. W., Anderson, H. R., Brunekreef, B., & Cassee, F. R. (2011). Black carbon as an additional indicator of the adverse health effects of airborne particles compared with PM10 and PM2. 5. *Environ Health Perspect, 119*(12), 1691-1699. doi:10.1289/ehp.1003369

Jimenez, J. L., Canagaratna, M. R., Donahue, N. M., Prevot, A. S. H., Zhang, Q., Kroll, J. H., DeCarlo, P. F., Allan, J. D., Coe, H., Ng, N. L., Aiken, A. C., Docherty, K. S., Ulbrich, I. M., Grieshop, A. P., Robinson, A. L., Duplissy, J., Smith, J. D., Wilson, K. R., Lanz, V. A., Hueglin, C., Sun, Y. L., Tian, J., Laaksonen, A., Raatikainen, T., Rautiainen, J., Vaattovaara, P., Ehn, M., Kulmala, M., Tomlinson, J. M., Collins, D. R., Cubison, M. J., Dunlea, J., Huffman, J. A., Onasch, T. B., Alfarra, M. R., Williams, P. I., Bower, K., Kondo, Y., Schneider, J., Drewnick, F., Borrmann, S., Weimer, S., Demerjian, K., Salcedo, D., Cottrell, L., Griffin, R., Takami, A.,

Miyoshi, T., Hatakeyama, S., Shimono, A., Sun, J. Y., Zhang, Y. M., Dzepina, K., Kimmel, J. R., Sueper, D., Jayne, J. T., Herndon, S. C., Trimborn, A. M., Williams, L. R., Wood, E. C., Middlebrook, A. M., Kolb, C. E., Baltensperger, U., & Worsnop, D. R. (2009). Evolution of Organic Aerosols in the Atmosphere. *Science, 326*(5959), 1525-1529. doi:10.1126/science.1180353

Järvinen, E., Virkkula, A., Nieminen, T., Aalto, P. P., Asmi, E., Lanconelli, C., Busetto, M., Lupi, A., Schioppo, R., Vitale, V., Mazzola, M., Petäjä, T., Kerminen, V. M., & Kulmala, M. (2013). Seasonal cycle and modal structure of particle number size distribution at Dome C, Antarctica. *Atmos Chem Phys, 13*(15), 7473-7487. doi:10.5194/acp-13-7473-2013

Kannosto, J., Lemmetty, M., Virtanen, A., Mäkelä, J., Keskinen, J., Junninen, H., Hussein, T., Aalto, P., & Kulmala, M. (2008). Mode resolved density of atmospheric aerosol particles. *Atmos Chem Phys Discuss, 8*(2), 7263-7288. doi:10.5194/acp-8-5327-2008

Karvosenoja, N., Kangas, L., Kupiainen, K., Kukkonen, J., Karppinen, A., Sofiev, M., Tainio, M., Paunu, V.-V., Ahtoniemi, P., & Tuomisto, J. T. (2011). Integrated modeling assessments of the population exposure in Finland to primary PM2. 5 from traffic and domestic wood combustion on the resolutions of 1 and 10 km. *Air Qual Atmos Hlth, 4*, 179-188. doi:10.1007/s11869-010-0100-9

Kerminen, V. M., Paramonov, M., Anttila, T., Riipinen, I., Fountoukis, C., Korhonen, H., Asmi, E., Laakso, L., Lihavainen, H., Swietlicki, E., Svenningsson, B., Asmi, A., Pandis, S. N., Kulmala, M., & Petäjä, T. (2012). Cloud condensation nuclei production associated with atmospheric nucleation: a synthesis based on existing literature and new results. *Atmos Chem Phys, 12*(24), 12037-12059. doi:10.5194/acp-12-12037-2012

Kirchstetter, T. W., Novakov, T., & Hobbs, P. V. (2004). Evidence that the spectral dependence of light absorption by aerosols is affected by organic carbon. *J Geophys Res-Atmos, 109*(D21). doi:10.1029/2004JD004999

Koch, D., & Del Genio, A. D. (2010). Black carbon semi-direct effects on cloud cover: review and synthesis. *Atmos Chem Phys, 10*(16), 7685-7696. doi:10.5194/acp-10-7685-2010

Koschmieder, H. (1924). Theorie der horizontalen Sichtweite. *Beiträge zur Physik der freien Atmosphäre*, 33-53.

Krecl, P., Johansson, C., Targino, A. C., Ström, J., & Burman, L. (2017). Trends in black carbon and size-resolved particle number concentrations and vehicle emission factors under real-world conditions. *Atmos Environ, 165*, 155-168. doi:10.1016/j.atmosenv.2017.06.036

Krzyżanowski, M., Kuna-Dibbert, B., & Schneider, J. (2005). *Health effects of transport-related air pollution*: WHO Regional Office Europe.

Kukkonen, J., López-Aparicio, S., Segersson, D., Geels, C., Kangas, L., Kauhaniemi, M., Maragkidou, A., Jensen, A., Assmuth, T., Karppinen, A., Sofiev, M., Hellén, H., Riikonen, K., Nikmo, J., Kousa, A., Niemi, J. V., Karvosenoja, N., Santos, G. S., Sundvor, I., Im, U., Christensen, J. H., Nielsen, O. K., Plejdrup, M. S., Nøjgaard, J. K., Omstedt, G., Andersson, C., Forsberg, B., & Brandt, J. (2020). The influence of residential wood combustion on the concentrations of PM2.5 in four Nordic cities. *Atmos Chem Phys, 20*(7), 4333-4365. doi:10.5194/acp-20-4333-2020

Kulmala, M. (2018). Build a global Earth observatory. *Nature, 553*, 21-23. doi:10.1038/d41586-017-08967-y

Kulmala, M., Kontkanen, J., Junninen, H., Lehtipalo, K., Manninen, H. E., Nieminen, T., Petäjä, T., Sipilä, M., Schobesberger, S., Rantala, P., Franchin, A., Jokinen, T., Järvinen, E., Äijälä, M., Kangasluoma, J., Hakala, J., Aalto, P. P., Paasonen, P., Mikkilä, J., Vanhanen, J., Aalto, J., Hakola, H., Makkonen, U., Ruuskanen, T., Mauldin, R. L., Duplissy, J., Vehkamäki, H., Bäck, J., Kortelainen, A., Riipinen, I., Kurtén, T., Johnston, M. V., Smith, J. N., Ehn, M., Mentel, T. F., Lehtinen, K. E. J., Laaksonen, A., Kerminen, V.-M., & Worsnop, D. R. (2013). Direct Observations of Atmospheric Aerosol Nucleation. *Science, 339*(6122), 943-946. doi:10.1126/science.1227385

Kulmala, M., Vehkamäki, H., Petäjä, T., Dal Maso, M., Lauri, A., Kerminen, V.-M., Birmili, W., & McMurry, P. (2004). Formation and growth rates of ultrafine atmospheric particles: A review of observations. *J Aerosol Sci, 35*(2), 143-176.

Kutzner, R. D., von Schneidemesser, E., Kuik, F., Quedenau, J., Weatherhead, E. C., & Schmale, J. (2018). Long-term monitoring of black carbon across Germany. *Atmos Environ, 185*, 41-52. doi:10.1016/j.atmosenv.2018.04.039

Laakso, L., Hussein, T., Aarnio, P., Komppula, M., Hiltunen, V., Viisanen, Y., & Kulmala, M. (2003). Diurnal and annual characteristics of particle mass and number concentrations in urban, rural and Arctic environments in Finland. *Atmos Environ, 37*(19), 2629-2641. doi:10.1016/S1352-2310(03)00206-1

Lack, D., & Cappa, C. (2010). Impact of brown and clear carbon on light absorption enhancement, single scatter albedo and absorption wavelength dependence of black carbon. *Atmos Chem Phys, 10*(9), 4207-4220. doi:10.5194/acp-10-4207-2010

Laj, P., Bigi, A., Rose, C., Andrews, E., Lund Myhre, C., Collaud Coen, M., Lin, Y., Wiedensohler, A., Schulz, M., Ogren, J. A., Fiebig, M., Gliß, J., Mortier, A., Pandolfi, M., Petäja, T., Kim, S. W., Aas, W., Putaud, J. P., Mayol-Bracero, O., Keywood, M., Labrador, L., Aalto, P., Ahlberg, E., Alados Arboledas, L., Alastuey, A., Andrade, M., Artíñano, B., Ausmeel, S., Arsov, T., Asmi, E., Backman, J., Baltensperger, U., Bastian, S., Bath, O., Beukes, J. P., Brem, B. T., Bukowiecki, N., Conil, S., Couret, C., Day, D., Dayantolis, W., Degorska, A., Eleftheriadis, K., Fetfatzis, P., Favez, O., Flentje, H., Gini, M. I., Gregorič, A., Gysel-Beer, M., Hallar, A. G., Hand, J., Hoffer, A., Hueglin, C., Hooda, R. K., Hyvärinen, A., Kalapov, I., Kalivitis, N., Kasper-Giebl, A., Kim, J. E., Kouvarakis, G., Kranjc, I., Krejci, R., Kulmala, M., Labuschagne, C., Lee, H. J., Lihavainen, H., Lin, N. H., Löschau, G., Luoma, K., Marinoni, A., Martins Dos Santos, S., Meinhardt, F., Merkel, M., Metzger, J. M., Mihalopoulos, N., Nguyen, N. A., Ondracek, J., Pérez, N., Perrone, M. R., Petit, J. E., Picard, D., Pichon, J. M., Pont, V., Prats, N., Prenni, A., Reisen, F., Romano, S., Sellegri, K., Sharma, S., Schauer, G., Sheridan, P., Sherman, J. P., Schütze, M., Schwerin, A., Sohmer, R., Sorribas, M., Steinbacher, M., Sun, J., Titos, G., Toczko, B., Tuch, T., Tulet, P., Tunved, P., Vakkari, V., Velarde, F., Velasquez, P., Villani, P., Vratolis, S., Wang, S. H., Weinhold, K., Weller, R., Yela, M., Yus-Diez, J., Zdimal, V., Zieger, P., & Zikova, N. (2020). A global analysis of climate-relevant aerosol properties retrieved from the network of Global Atmosphere Watch (GAW) near-surface observatories. *Atmos Meas Tech, 13*(8), 4353-4392. doi:10.5194/amt-13-4353-2020

Lelieveld, J., Evans, J. S., Fnais, M., Giannadaki, D., & Pozzer, A. (2015). The contribution of outdoor air pollution sources to premature mortality on a global scale. *Nature, 525*(7569), 367–371. doi:10.1038/nature15371

Li, H., McMeeking, G. R., & May, A. A. (2020). Development of a new correction algorithm applicable to any filter-based absorption photometer. *Atmos Meas Tech, 13*(5), 2865-2886. doi:10.5194/amt-13-2865-2020

Li, J., Carlson, B. E., Dubovik, O., & Lacis, A. A. (2014). Recent trends in aerosol optical properties derived from AERONET measurements. *Atmos Chem Phys, 14*(22), 12271-12289. doi:10.5194/acp-14-12271-2014

Lihavainen, H., Hyvärinen, A., Asmi, E., Hatakka, J., & Viisanen, Y. (2015). Long-term variability of aerosol optical properties in northern Finland. *Boreal Environ Res, 20*, 526-541.

Liu, C., Chung, C. E., Yin, Y., & Schnaiter, M. (2018). The absorption Ångström exponent of black carbon: from numerical aspects. *Atmos Chem Phys, 18*(9), 6259-6273. doi:10.5194/acp-18-6259-2018

Liu, D., Whitehead, J., Alfarra, M. R., Reyes-Villegas, E., Spracklen, Dominick V., Reddington, Carly L., Kong, S., Williams, Paul I., Ting, Y.-C., Haslett, S., Taylor, Jonathan W., Flynn, Michael J., Morgan, William T., McFiggans, G., Coe, H., & Allan, James D. (2017). Black-carbon absorption enhancement in the atmosphere determined by particle mixing state. *Nature Geoscience, 10*(3), 184-188. doi:10.1038/ngeo2901

Lohmann, U., & Feichter, J. (2005). Global indirect aerosol effects: A review. *Atmos Chem Phys, 5*(3), 715-737. doi:10.5194/acp-5-715-2005

McMurry, P. H. (2000). A review of atmospheric aerosol measurements. *Atmos Environ, 34*(12-14), 1959-1999. doi:10.1016/S1352-2310(99)00455-0

Moise, T., Flores, J. M., & Rudich, Y. (2015). Optical Properties of Secondary Organic Aerosols and Their Changes by Chemical Processes. *Chem Rev, 115*(10), 4400-4439. doi:10.1021/cr5005259

Moosmüller, H., Chakrabarty, R. K., & Arnott, W. P. (2009). Aerosol light absorption and its measurement: A review. *J Quant Spectrosc Radiat Transfer, 110*(11), 844-878. doi:10.1016/j.jqsrt.2009.02.035

Moteki, N., Kondo, Y., Nakayama, T., Kita, K., Sahu, L. K., Ishigai, T., Kinase, T., & Matsumi, Y. (2010). Radiative transfer modeling of filter-based measurements of light absorption by particles: Importance of particle size dependent penetration depth. *J Aerosol Sci, 41*(4), 401-412. doi:10.1016/j.jaerosci.2010.02.002

Myhre, G., Shindell, D., Bréon, F., Collins, W., Fuglestvedt, J., Huang, J., Koch, D., Lamarque, J., Lee, D., Mendoza, B., Nakajima, T., Robock, A., Stephens, G., Takemura, T., & Zhang, H. (2013). *Anthropogenic and natural radiative forcing, In: Climate Change 2013: The Physical Science Basis. Contribution of Working Group I to the Fifth Assessment Report of the Intergovernmental Panel on Climate Change [Stocker, T.F., D. Qin, G.-K. Plattner, M. Tignor, S.K. Allen, J. Boschung, A. Nauels, Y. Xia, V. Bex and P.M. Midgley (eds.)]*. (1107415322).

Müller, T., Laborde, M., Kassell, G., & Wiedensohler, A. (2011). Design and performance of a three-wavelength LED-based total scatter and backscatter integrating nephelometer. *Atmos Meas Tech, 4*(6), 1291-1303. doi:10.5194/amt-4-1291-2011

Mätzler, C. (2002). *MATLAB functions for Mie scattering and absorption, version 2*. Bern.

Ogren, J. A. (2010). Comment on "Calibration and intercomparison of filter-based measurements of visible light absorption by aerosols". *Aerosol Sci Technol, 44*(8), 589-591. doi:10.1080/02786826.2010.482111

Paasonen, P., Kupiainen, K., Klimont, Z., Visschedijk, A., Denier van der Gon, H. A. C., & Amann, M. (2016). Continental anthropogenic primary particle number emissions. *Atmos Chem Phys, 16*(11), 6823-6840. doi:10.5194/acp-16-6823-2016

Pandolfi, M., Alados-Arboledas, L., Alastuey, A., Andrade, M., Angelov, C., Artiñano, B., Backman, J., Baltensperger, U., Bonasoni, P., & Bukowiecki, N. (2018). A European aerosol phenomenology–6: Scattering properties of atmospheric aerosol particles from 28 ACTRIS sites. *Atmos Chem Phys, 18*(11), 7877-7911. doi:10.5194/acp-18-7877-2018

Peng, J., Hu, M., Guo, S., Du, Z., Zheng, J., Shang, D., Levy Zamora, M., Zeng, L., Shao, M., Wu, Y.-S., Zheng, J., Wang, Y., Glen, C. R., Collins, D. R., Molina, M. J., & Zhang, R. (2016). Markedly enhanced absorption and direct radiative forcing of black carbon under polluted urban environments. *Proceedings of the National Academy of Sciences, 113*(16), 4266-4271. doi:10.1073/pnas.1602310113

Perrin, F. H. (1948). Whose absorption law? *J Opt Soc Am, 38*(1), 72-74. doi:10.1364/JOSA.38.000072

Petzold, A., Ogren, J. A., Fiebig, M., Laj, P., Li, S.-M., Baltensperger, U., Holzer-Popp, T., Kinne, S., Pappalardo, G., Sugimoto, N., Wehrli, C., Wiedensohler, A., & Zhang, X.-Y. (2013). Recommendations for reporting "black carbon" measurements. *Atmos Chem Phys, 13*(16), 8365-8379. doi:10.5194/acp-13-8365-2013

Petzold, A., & Schönlinner, M. (2004). Multi-angle absorption photometry—a new method for the measurement of aerosol light absorption and atmospheric black carbon. *J Aerosol Sci, 35*(4), 421-441. doi:10.1016/j.jaerosci.2003.09.005

Qi, X. M., Ding, A. J., Nie, W., Petäjä, T., Kerminen, V. M., Herrmann, E., Xie, Y. N., Zheng, L. F., Manninen, H., Aalto, P., Sun, J. N., Xu, Z. N., Chi, X. G., Huang, X., Boy, M., Virkkula, A., Yang, X. Q., Fu, C. B., & Kulmala, M. (2015). Aerosol size distribution and new particle formation in the western Yangtze River Delta of China: 2 years of measurements at the SORPES station. *Atmos Chem Phys, 15*(21), 12445-12464. doi:10.5194/acp-15-12445-2015

Ramanathan, V., & Carmichael, G. (2008). Global and regional climate changes due to black carbon. *Nature Geoscience, 1*(4), 221-227. doi:10.1038/ngeo156

Rautalahti, E., & Kupiainen, K. (2016). *Emissions of black carbon and methane in Finland*. Helsinki.

Rodríguez, S., & Cuevas, E. (2007). The contributions of “minimum primary emissions” and “new particle formation enhancements” to the particle number concentration in urban air. *J Aerosol Sci, 38*(12), 1207-1219. doi:10.1016/j.jaerosci.2007.09.001

Rönkkö, T., & Timonen, H. (2019). Overview of sources and characteristics of nanoparticles in urban traffic-influenced areas. *J Alzheimer's Dis, 72*, 15-28. doi:10.3233/JAD-190170

Sandradewi, J., Prévôt, A. S., Szidat, S., Perron, N., Alfarra, M. R., Lanz, V. A., Weingartner, E., & Baltensperger, U. (2008). Using aerosol light absorption measurements for the quantitative determination of wood burning and traffic emission contributions to particulate matter. *Environ Sci Technol, 42*(9), 3316-3323. doi:10.1021/es702253m

Saturno, J., Pöhlker, C., Massabò, D., Brito, J., Carbone, S., Cheng, Y., Chi, X., Ditas, F., Hrabě de Angelis, I., Morán-Zuloaga, D., Pöhlker, M. L., Rizzo, L. V., Walter, D., Wang, Q., Artaxo, P., Prati, P., & Andreae, M. O. (2017). Comparison of different Aethalometer correction schemes and a reference multi-wavelength absorption technique for ambient aerosol data. *Atmos Meas Tech, 10*(8), 2837-2850. doi:10.5194/amt-10-2837-2017

Savolahti, M., Karvosenoja, N., Tissari, J., Kupiainen, K., Sippula, O., & Jokiniemi, J. (2016). Black carbon and fine particle emissions in Finnish residential wood combustion: Emission projections, reduction measures and the impact of

combustion practices. *Atmos Environ, 140*, 495-505. doi:10.1016/j.atmosenv.2016.06.023

Schmid, O., Artaxo, P., Arnott, W. P., Chand, D., Gatti, L. V., Frank, G. P., Hoffer, A., Schnaiter, M., & Andreae, M. O. (2006). Spectral light absorption by ambient aerosols influenced by biomass burning in the Amazon Basin. I: Comparison and field calibration of absorption measurement techniques. *Atmos Chem Phys, 6*(11), 3443-3462. doi:10.5194/acp-6-3443-2006

Schraufnagel, D. E., Balmes, J. R., Cowl, C. T., De Matteis, S., Jung, S.-H., Mortimer, K., Perez-Padilla, R., Rice, M. B., Riojas-Rodriguez, H., Sood, A., Thurston, G. D., To, T., Vanker, A., & Wuebbles, D. J. (2019). Air Pollution and Noncommunicable Diseases: A Review by the Forum of International Respiratory Societies' Environmental Committee, Part 1: The Damaging Effects of Air Pollution. *Chest, 155*(2), 409-416. doi:10.1016/j.chest.2018.10.042

Schuster, G. L., Dubovik, O., & Holben, B. N. (2006). Angstrom exponent and bimodal aerosol size distributions. *J Geophys Res-Atmos, 111*(D7). doi:10.1029/2005JD006328

Seinfeld, J. H., & Pandis, S. N. (2016). *Atmospheric chemistry and physics: from air pollution to climate change*: John Wiley & Sons.

Shen, H., Huang, Y., Wang, R., Zhu, D., Li, W., Shen, G., Wang, B., Zhang, Y., Chen, Y., Lu, Y., Chen, H., Li, T., Sun, K., Li, B., Liu, W., Liu, J., & Tao, S. (2013). Global Atmospheric Emissions of Polycyclic Aromatic Hydrocarbons from 1960 to 2008 and Future Predictions. *Environmental Science & Technology, 47*(12), 6415-6424. doi:10.1021/es400857z

Shen, Y., Virkkula, A., Ding, A., Wang, J., Chi, X., Nie, W., Qi, X., Huang, X., Liu, Q., Zheng, L., Zheng, X., Petäjä, T., Aalto, P., Fu, C., & Kulmala, M. (2018). Aerosol optical properties at SORPES in Nanjing, east China. *Atmos Chem Phys, 18*(8), 5265-5292. doi:10.5194/acp-18-5265-2018

Sheridan, P. J., & Ogren, J. A. (1999). Observations of the vertical and regional variability of aerosol optical properties over central and eastern North America. *J Geophys Res-Atmos, 104*(D14), 16793-16805.

Sherman, J., Sheridan, P., Ogren, J., Andrews, E., Hageman, D., Schmeisser, L., Jefferson, A., & Sharma, S. (2015). A multi-year study of lower tropospheric aerosol variability and systematic relationships from four North American regions. *Atmos Chem Phys, 15*(21), 12487-12517. doi:10.5194/acp-15-12487-2015

Singh, V., Ravindra, K., Sahu, L., & Sokhi, R. (2018). Trends of atmospheric black carbon concentration over the United Kingdom. *Atmos Environ, 178*, 148-157. doi:10.1016/j.atmosenv.2018.01.030

Stocker, T. F., Qin, D., Plattner, G.-K., Tignor, M., Allen, S. K., Boschung, J., Nauels, A., Xia, Y., Bex, V., & Midgley, P. M. (2013). *Climate change 2013: The physical science basis*.

Sun, J., Birmili, W., Hermann, M., Tuch, T., Weinhold, K., Merkel, M., Rasch, F., Müller, T., Schladitz, A., Bastian, S., Löschau, G., Cyrys, J., Gu, J., Flentje, H., Briel, B., Asbach, C., Kaminski, H., Ries, L., Sohmer, R., Gerwig, H., Wirtz, K., Meinhardt, F., Schwerin, A., Bath, O., Ma, N., & Wiedensohler, A. (2020). Decreasing trends of particle number and black carbon mass concentrations at 16 observational sites in Germany from 2009 to 2018. *Atmos Chem Phys, 20*(11), 7049-7068. doi:10.5194/acp-20-7049-2020

Tang, I. N. (1996). Chemical and size effects of hygroscopic aerosols on light scattering coefficients. *J Geophys Res-Atmos, 101*(D14), 19245-19250. doi:10.1029/96JD03003

Teinilä, K., Aurela, M., Niemi, J. V., Kousa, A., Petäjä, T., Järvi, L., Hillamo, R., Kangas, L., Saarikoski, S., & Timonen, H. (2019). Concentration variation of gaseous and particulate pollutants in the Helsinki city centre — observations from a two-year campaign from 2013–2015. *Boreal Environ Res, 24*, 115-136.

Titos, G., Lyamani, H., Drinovec, L., Olmo, F. J., Močnik, G., & Alados-Arboledas, L. (2015). Evaluation of the impact of transportation changes on air quality. *Atmos Environ, 114*, 19-31. doi:10.1016/j.atmosenv.2015.05.027

Twomey, S. (1991). Aerosols, clouds and radiation. *Atmospheric Environment. Part A. General Topics, 25*(11), 2435-2442. doi:10.1016/0960-1686(91)90159-5

Wagstrom, K. M., & Pandis, S. N. (2009). Determination of the age distribution of primary and secondary aerosol species using a chemical transport model. *J Geophys Res-Atmos, 114*(D14). doi:10.1029/2009JD011784

Valavanidis, A., Fiotakis, K., & Vlachogianni, T. (2008). Airborne Particulate Matter and Human Health: Toxicological Assessment and Importance of Size and Composition of Particles for Oxidative Damage and Carcinogenic Mechanisms. *Journal of Environmental Science and Health, Part C, 26*(4), 339-362. doi:10.1080/10590500802494538

Weingartner, E., Saathoff, H., Schnaiter, M., Streit, N., Bitnar, B., & Baltensperger, U. (2003). Absorption of light by soot particles: determination of the absorption coefficient by means of Aethalometers. *J Aerosol Sci, 34*(10), 1445-1463. doi:10.1016/S0021-8502(03)00359-8

WHO. (2012). *Health effects of black carbon*: WHO.

WHO. (2016). WHO Global Urban Ambient Air Pollution Database. Retrieved from https://www.who.int/phe/health_topics/outdoorair/databases/cities/en/

Vicente, E. D., & Alves, C. A. (2018). An overview of particulate emissions from residential biomass combustion. *Atmos Res, 199*, 159-185. doi:10.1016/j.atmosres.2017.08.027

Virkkula, A. (2010). Correction of the calibration of the 3-wavelength particle soot absorption photometer (3λ PSAP). *Aerosol Sci Technol, 44*(8), 706-712. doi:10.1080/02786826.2010.482110

Virkkula, A., Ahlquist, N. C., Covert, D. S., Arnott, W. P., Sheridan, P. J., Quinn, P. K., & Coffman, D. J. (2005). Modification, calibration and a field test of an instrument for measuring light absorption by particles. *Aerosol Sci Technol, 39*(1), 68-83. doi:10.1080/027868290901963

Virkkula, A., Backman, J., Aalto, P., Hulkkonen, M., Riuttanen, L., Nieminen, T., Dal Maso, M., Sogacheva, L., De Leeuw, G., & Kulmala, M. (2011). Seasonal cycle, size dependencies, and source analyses of aerosol optical properties at the SMEAR II measurement station in Hyytiala, Finland. *Atmos Chem Phys, 11*(9), 4445–4468. doi:10.5194/acp-11-4445-2011

Virkkula, A., Mäkelä, T., Hillamo, R., Yli-Tuomi, T., Hirsikko, A., Hämeri, K., & Koponen, I. K. (2007). A simple procedure for correcting loading effects of Aethalometer data. *J Air Waste Ma, 57*(10), 1214-1222. doi:10.3155/1047-3289.57.10.1214

WMO/GAW. (2016). *Aerosol measurement procedures, guidelines and recommendations, 2nd edition, GAW Report No. 227*.

Zhang, Q., Jimenez, J. L., Canagaratna, M. R., Allan, J. D., Coe, H., Ulbrich, I., Alfarra, M. R., Takami, A., Middlebrook, A. M., Sun, Y. L., Dzepina, K., Dunlea, E., Docherty, K., DeCarlo, P. F., Salcedo, D., Onasch, T., Jayne, J. T., Miyoshi, T., Shimono, A.,

Hatakeyama, S., Takegawa, N., Kondo, Y., Schneider, J., Drewnick, F., Borrmann, S., Weimer, S., Demerjian, K., Williams, P., Bower, K., Bahreini, R., Cottrell, L., Griffin, R. J., Rautiainen, J., Sun, J. Y., Zhang, Y. M., & Worsnop, D. R. (2007). Ubiquity and dominance of oxygenated species in organic aerosols in anthropogenically-influenced Northern Hemisphere midlatitudes. *Geophys Res Lett, 34*(13). doi:10.1029/2007GL029979

Zhang, R., Khalizov, A. F., Pagels, J., Zhang, D., Xue, H., & McMurry, P. H. (2008). Variability in morphology, hygroscopicity, and optical properties of soot aerosols during atmospheric processing. *Proc Natl Acad Sci USA, 105*(30), 10291-10296. doi:10.1073/pnas.0804860105

Zhao, B., Jiang, J. H., Gu, Y., Diner, D., Worden, J., Liou, K.-N., Su, H., Xing, J., Garay, M., & Huang, L. (2017). Decadal-scale trends in regional aerosol particle properties and their linkage to emission changes. *Environ Res Lett, 12*(5), 054021. doi:10.1088/1748-9326/aa6cb2

Zieger, P., Aalto, P., Aaltonen, V., Äijälä, M., Backman, J., Hong, J., Komppula, M., Krejci, R., Laborde, M., & Lampilahti, J. (2015). Low hygroscopic scattering enhancement of boreal aerosol and the implications for a columnar optical closure study. *Atmos Chem Phys, 15*(13), 7247-7267.

Ziemann, P. J., & Atkinson, R. (2012). Kinetics, products, and mechanisms of secondary organic aerosol formation. *Chem Soc Rev, 41*(19), 6582-6605. doi:10.1039/C2CS35122F

Zotter, P., Herich, H., Gysel, M., El-Haddad, I., Zhang, Y., Močnik, G., Hüglin, C., Baltensperger, U., Szidat, S., & Prévôt, A. S. (2017). Evaluation of the absorption Ångström exponents for traffic and wood burning in the Aethalometer-based source apportionment using radiocarbon measurements of ambient aerosol. *Atmos Chem Phys, 17*(6), 4229-4249. doi:10.5194/acp-17-4229-2017

Ångström, A. (1929). On the atmospheric transmission of sun radiation and on dust in the air. *Geografiska Annaler, 11*(2), 156-166. doi:10.2307/519399